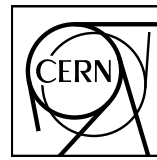


EUROPEAN ORGANIZATION FOR NUCLEAR RESEARCH



ALICE



CERN-EP-2025-137

14 June 2025

Medium-induced modification of azimuthal correlations of electrons from heavy-flavor hadron decays with charged particles in Pb–Pb collisions at

$$\sqrt{s_{\text{NN}}} = \mathbf{5.02 \text{ TeV}}$$

ALICE Collaboration*

Abstract

The azimuthal-correlation distributions between electrons from the decays of heavy-flavor hadrons and associated charged particles in Pb–Pb collisions at $\sqrt{s_{\text{NN}}} = 5.02 \text{ TeV}$ are reported for the 0–10% and 30–50% centrality classes. This is the first measurement to provide access to the azimuthal-correlation observables in the heavy-flavor sector in Pb–Pb collisions. The analysis is performed for trigger electrons from heavy-flavor hadron decays with transverse momentum $4 < p_T^e < 16 \text{ GeV}/c$, considering associated particles within the transverse-momentum range $1 < p_T^{\text{assoc}} < 7 \text{ GeV}/c$, and a pseudorapidity difference of $|\Delta\eta| < 1$ between the trigger electron and associated particles. The per-trigger nuclear modification factor (I_{AA}) is calculated to compare the near- and away-side peak yields to those in pp collisions at $\sqrt{s} = 5.02 \text{ TeV}$. In 0–10% central collisions, the I_{AA} indicates a hint of enhancement of associated-particle yields with $p_T < 3 \text{ GeV}/c$ on the near side, and a suppression of yields with $p_T > 4 \text{ GeV}/c$ on the away side. The I_{AA} for electron triggers from heavy-flavor hadron decays is compared with that for light-flavor and strange-particle triggers to investigate the dependence on different fragmentation processes and parton-medium dynamics, and is found to be the same within uncertainties.

© 2025 CERN for the benefit of the ALICE Collaboration.

Reproduction of this article or parts of it is allowed as specified in the CC-BY-4.0 license.

*See Appendix B for the list of collaboration members

1 Introduction

In hadronic collisions, heavy quarks are produced in hard-scattering processes, with large squared-momentum transfer, Q^2 [1–4]. High-energy partons produced in such hard scatterings radiate gluons, generating a parton shower. The shower hadronizes, producing a collimated spray of particles called a jet. Jet-reconstruction algorithms [5, 6] can be used to study their production and substructure, which provide stringent tests of perturbative quantum chromodynamics (pQCD) calculations. Two-particle angular correlations are a complementary method to jet-reconstruction measurements for characterizing jet properties, especially at low p_T [7, 8]. The typical features of a two-particle angular-correlation distribution of trigger particles with associated charged particles are a “near-side” (NS) peak at $(\Delta\phi, \Delta\eta) \approx (0, 0)$ and an “away-side” (AS) peak at $\Delta\phi \approx \pi$, which extends over a wide pseudorapidity range [9–11]. At leading order (LO) accuracy in vacuum QCD, the NS peak originates primarily from particles emerging from the fragmentation of the same parton that produced the trigger particle [12]. The AS peak is related to the fragmentation of the other outgoing parton produced in the hard scattering [12]. Next-to-leading order (NLO) processes, such as gluon radiation, gluon splitting, or flavor excitation [13] can alter the LO topology of the correlation shapes [11–13]. Angular correlation measurements with a heavy-flavor particle trigger facilitate the study of heavy-flavor jet properties. By varying the p_T intervals of the trigger and associated particles, the details of jet fragmentation can be investigated, such as the jet angular profile and the momentum distribution of the particles produced in the hard-parton fragmentation.

In ultrarelativistic heavy-ion collisions, a deconfined phase of strongly-interacting matter is produced, known as quark–gluon plasma (QGP) [14–18]. Experiments at the CERN Large Hadron Collider (LHC) [19, 20] and the Brookhaven Relativistic Heavy Ion Collider (RHIC) [21–24] have extensively studied the properties of the QGP, characterizing it as a near-perfect liquid with very low specific shear viscosity-to-entropy ratio. One of the signatures of QGP is the parton energy loss, where high-energy partons traversing this medium lose energy due to medium-induced gluon radiation and collisions with medium constituents [25–30]. This results in reduced energy for the parton showers producing a jet, referred to as “jet quenching”. In this process, the particle distribution within the jet undergoes modification, changing the internal structure of the jet, thus affecting the fragmentation function [31, 32]. A previous measurement of the jet fragmentation function shows modifications in Pb–Pb collisions compared to pp collisions, with an excess of low- p_T particles in inclusive jets [33–36]. High-momentum partons propagating through the QGP medium can also lead to modifications in the QGP itself due to the injection of energy and momentum lost by the jet into the plasma [37]. This yields a correlation between the bulk dynamics of the medium and the jet [38–41]. Measurements of heavy-flavor jets and particle distributions within jets can serve to constrain parton energy-loss mechanisms and probe how the lost energy is redistributed among other partons and subsequent particles emerging from the collision. Theoretical models predict that energy loss depends on the quark mass and the color charge of the parton [26–28, 42]. Heavy quarks are expected to lose less energy than light quarks [27, 28, 42], which is corroborated by measurements of the nuclear modification factor (R_{AA}) of charm and beauty hadrons [43–49], and jets containing heavy-flavor particles [50–52].

Measurements of two-particle angular correlations using light-flavor hadrons as trigger particles are employed by the ALICE Collaboration [7, 8, 53] to study jet quenching in Pb–Pb collisions. These measurements indicate a strong suppression of the per-trigger AS peak yield at high associated-particle p_T , and an enhancement of the low- p_T associated-particle yield on the near side in central Pb–Pb collisions compared to pp collisions. Moreover, the measurement of charged-particle jets recoiling from a high- p_T parton [54, 55] shows a strong medium-induced enhancement of recoil jets at low $p_{T,jet}$ in Pb–Pb collisions compared to pp collisions. This enhancement potentially arises from the response of the QGP medium to jets, as described by calculations which incorporate such a medium response [56]. Measurements of the angular correlations using heavy-flavor hadrons as trigger particles, and studying their peak yield modifications, can expand the investigation of jet transport and QGP dynamics in the heavy-flavor

sector, allowing for further exploration of the parton mass dependence of parton–medium interactions. The PHENIX and STAR Collaborations at RHIC conducted studies of angular correlations of electrons from heavy-flavor hadron decays with charged hadrons [57] and angular correlations of D mesons with charged hadrons [58] in Au–Au collisions at $\sqrt{s_{\text{NN}}} = 200$ GeV. Although these correlation measurements are statistically limited, they indicate modifications of the NS and AS correlation peaks in central Au–Au collisions compared to pp collisions, suggesting QGP effects. The CMS Collaboration investigated the modification of the jet profile initiated by beauty quarks (b jets) [52]. The measurement illustrates a redistribution of the p_{T} of jet constituents from small to large distances from the jet axis. A large-distance enhancement is observed in Pb–Pb collisions, more pronounced for b jets than for inclusive jets, indicating mass-dependent interactions in the QGP.

This article presents the first measurement of jet-like correlations in Pb–Pb collisions at LHC energies using a particle from the heavy-flavor sector as the trigger particle. The study is based on azimuthal-correlation distributions between electrons from heavy-flavor hadron decays and associated charged particles in Pb–Pb collisions at $\sqrt{s_{\text{NN}}} = 5.02$ TeV, conducted using the ALICE detector. The correlation distributions are studied for various p_{T} intervals of both trigger electrons and associated charged particles to explore the p_{T} dependence of the correlation shapes. The results are compared with those measured in pp collisions at the same center-of-mass energy [11] to investigate the effects of the QGP medium on the particle distribution within the heavy-flavor jet.

The article is organized as follows. The ALICE apparatus, its main detectors used in the analyses, and the data samples are reported in Sec. 2. The complete analysis procedure is described in Sec. 3. The systematic uncertainties associated with the measurements are discussed in Sec. 4. The analysis results are presented and discussed in Sec. 5. The article is briefly summarized in Sec. 6.

2 Experimental apparatus and data sample

The measurement is performed with the ALICE detector at the LHC. A complete description of the ALICE detector is detailed in Refs. [59, 60]. The central barrel of the detector is located at midrapidity ($|\eta| < 0.9$) and is embedded within a cylindrical solenoid that produces a magnetic field of 0.5 T parallel to the direction of the beam. The main detectors used for this analysis are the Inner Tracking System (ITS), the Time Projection Chamber (TPC), the electromagnetic calorimeters (EMCal and DCal), the V0, and the Zero Degree Calorimeters (ZDC). The ITS [61] is used for the reconstruction of the primary vertex and charged-particle tracking. It consists of six cylindrical layers of silicon detectors, with the innermost two layers composed of Silicon Pixel Detectors (SPD), the middle two made of Silicon Drift Detectors, and the outer layers composed of Silicon Strip Detectors. The TPC [62] is the core of the ALICE tracking system, providing three-dimensional information of particle momenta as well as specific energy loss (dE/dx) measurements for the purpose of charged-particle identification [63–65]. The EMCal ($|\eta| < 0.7$ and $80^\circ < \phi < 187^\circ$) and DCal ($0.22 < |\eta| < 0.7$ and $260^\circ < \phi < 320^\circ$, $|\eta| < 0.7$ and $320^\circ < \phi < 327^\circ$) detectors [66, 67] are used for electron identification and event triggering. The EMCal and DCal detectors will be collectively referred to as EMCal for the remainder of this paper. The V0 system is used for centrality estimation [68] and is composed of two scintillator arrays, V0A and V0C, which cover the pseudorapidity ranges of $2.8 < \eta < 5.1$ and $-3.7 < \eta < -1.7$, respectively. Simultaneous signals in both the V0A and V0C detectors define the minimum-bias interaction (MB) trigger. The ZDC [69], located at 112.5 m on both sides of the interaction point, are utilized for rejecting electromagnetic interactions and beam-induced background in Pb–Pb collisions.

The results presented in this paper are obtained from Pb–Pb collisions at the center-of-mass energy of $\sqrt{s_{\text{NN}}} = 5.02$ TeV recorded during the LHC Run 2 and selected using the MB trigger of the 2018 run exploiting the V0 detector. Two centrality percentile classes [70] are used: 0–10%, classified as the most-central collision events, and 30–50%, categorized as semicentral collision events. Pileup events with two

or more primary vertices are rejected via an algorithm that detects multiple vertices reconstructed by the SPD. For the purpose of maintaining uniform acceptance, only collisions with a reconstructed primary vertex within ± 10 cm from the nominal interaction point ($z = 0$) along the beam axis are selected. The number of events analyzed is 41.5×10^6 (62.3×10^6) in 0–10% (30–50%) central (semicentral) Pb–Pb collisions, corresponding to an integrated luminosity of approximately $54 \mu\text{b}^{-1}$ ($41 \mu\text{b}^{-1}$) [70], respectively.

3 Analysis procedure

The analysis is performed by evaluating the two-particle azimuthal-correlation distributions between trigger electrons (and positrons) from heavy-flavor hadron decays [71] and associated charged primary particles. Particles are defined as primary if they have a mean proper lifetime $\tau > 1 \text{ cm}/c$ and are produced directly in the collision. A particle is also classified as primary if its parent has $\tau < 1 \text{ cm}/c$ and the parent originates from a decay chain arising from the collision. Secondary particles are those that do not meet the criteria for being classified as primaries [72]. Effects on the measured correlation distribution, induced by the detector’s limited acceptance and local inhomogeneities, are corrected using an event-mixing technique. The correlation distributions are normalized by the number of electron triggers and corrected for the associated-particle tracking efficiency. The contamination from hadrons misidentified as electrons, electrons from background sources, as well as secondary associated particles, are subtracted statistically from the measured distributions as it will be discussed below. The per-trigger peak yields are obtained after subtracting the contribution from uncorrelated pairs, referred to as baseline. The following section details the analysis procedure, which largely follows the procedure used in the measurement of angular correlations of electrons from heavy-flavor hadron decays and charged hadrons in pp and p–Pb collisions at $\sqrt{s_{\text{NN}}} = 5.02 \text{ TeV}$ [11]. Both positrons and electrons from heavy-flavor hadron decays will be collectively referred to as “electrons” for the remainder of this paper.

3.1 Electron identification and associated-particle reconstruction

Electron tracks with transverse momentum within $4 < p_T^e < 16 \text{ GeV}/c$ and within a pseudorapidity interval of $|\eta| < 0.6$ are considered. Track quality selections are applied by requiring the same selection criteria defined in Ref. [11, 73], and at least one hit in the SPD. To reject secondary electrons, which are produced from interactions with the detector material or from the weak decays of long-lived particles, a distance of closest approach requirement is imposed using the same selections as Ref. [11]. Particle identification is implemented by imposing a dE/dx selection on the TPC track and via the energy deposition in the EMCal detector. The discriminant variable for the TPC electron identification is the number of standard deviations ($n\sigma_e^{\text{TPC}}$) of the measured dE/dx from the expected value for electrons obtained from the Bethe-Bloch parameterization [63]. An asymmetric selection of $-1 < n\sigma_e^{\text{TPC}} < 3$ is applied due to the larger hadron background contamination in the region of negatively valued $n\sigma_e^{\text{TPC}}$. The ratio of the energy (E) deposited in the EMCal to the momentum (p) measured by the TPC provides another method of electron identification. Electrons produce an electromagnetic shower in the EMCal and deposit their total energy E . Because of their small mass relative to their momentum, their E/p ratio is very close to 1. The electron identification with the EMCal is thus performed by selecting candidates with $0.8 < E/p < 1.2$. In addition, the shape of the electromagnetic shower in the EMCal is used for electron identification and to reduce hadron contamination. The shower shape is characterized by the eigenvalues of the dispersion matrix of the shower shape ellipse defined by the energy distribution within the EMCal cluster [74, 75]. A long-axis selection of $0.02 < \sigma_{\text{long}}^2 < 0.9$ is used in the analysis.

Charged primary particles [72] (defined as “associated particles”) are correlated with the trigger particle within $|\eta| < 0.8$. The reconstruction of charged primary particles follows the same criteria as those in Ref. [11]. Track quality selections include requirements on the minimum number of crossed TPC pad rows and the minimum ratio of crossed TPC pad rows to findable clusters. Additionally, a minimum

DCA requirement is imposed.

The associated particles are required to have a smaller p_T than the trigger electron when selecting trigger–associated pair candidates, following the same requirement used in the pp and p–Pb analyses [11], which introduces a kinematic bias in the p_T intervals where p_T^{trig} and p_T^{assoc} overlap. This bias is reproduced by simulations and model predictions.

3.2 Azimuthal-correlation distribution and mixed-event correction

A two-dimensional correlation distribution, $C(\Delta\eta, \Delta\phi)$, is evaluated as a function of the azimuthal-angle difference ($\Delta\phi$) and the pseudorapidity difference ($\Delta\eta$) between trigger and associated particles. This distribution is computed for trigger p_T intervals $4 < p_T^e < 12 \text{ GeV}/c$, as well as $4 < p_T^e < 7 \text{ GeV}/c$ and $7 < p_T^e < 16 \text{ GeV}/c$, in each case for five associated p_T intervals between 1 and 7 GeV/c : $1 < p_T^{\text{assoc}} < 2 \text{ GeV}/c$, $2 < p_T^{\text{assoc}} < 3 \text{ GeV}/c$, $3 < p_T^{\text{assoc}} < 4 \text{ GeV}/c$, $4 < p_T^{\text{assoc}} < 5 \text{ GeV}/c$, and $5 < p_T^{\text{assoc}} < 7 \text{ GeV}/c$. These trigger and associated p_T intervals are selected to facilitate direct comparisons to the equivalent measurement in pp collisions [11]. The correlation distributions are corrected for pair acceptance and detector inhomogeneities for each p_T interval using a mixed-event technique as described in Ref. [76]. Equation 1 shows the mixed-event correction procedure, where $S(\Delta\eta, \Delta\phi)$ represents the two-dimensional correlation distribution after correction by the normalized mixed-event distribution $\frac{1}{\beta}ME(\Delta\eta, \Delta\phi)$.

$$\frac{d^2N}{d\Delta\eta d\Delta\phi} \equiv S(\Delta\eta, \Delta\phi) = \beta \times \frac{C(\Delta\eta, \Delta\phi)}{ME(\Delta\eta, \Delta\phi)} \quad (1)$$

The mixed-event correlation distribution, $ME(\Delta\eta, \Delta\phi)$, is constructed by correlating trigger electrons with associated charged particles from different collisions that have similar multiplicity and primary-vertex position along the beam axis as the events containing the electron. The resulting mixed-event correlation distribution is characterized by a triangular shape along the $\Delta\eta$ axis, due to the limited η coverage, and is approximately flat in $\Delta\phi$. In the region $(\Delta\eta, \Delta\phi) \approx (0, 0)$, the trigger and associated particles cross the same detector elements, therefore this region of the correlation distribution is not significantly affected by detector inhomogeneities. This property is used to obtain a normalization factor, β , for $ME(\Delta\eta, \Delta\phi)$. The β factor is defined as the average number of correlated pairs within $-0.2 < \Delta\phi < 0.2$ and $-0.07 < \Delta\eta < 0.07$ in the mixed-event correlation. To reduce the effect of statistical fluctuations, particularly at large $|\Delta\eta|$, the mixed-event corrected two-dimensional distribution, $S(\Delta\eta, \Delta\phi)$, is integrated over the pseudorapidity range of $|\Delta\eta| < 1$ to obtain a one-dimensional distribution $S(\Delta\phi)$.

3.3 Background subtraction

To obtain the final electron correlation distribution, two types of background must be removed from the electron signal: hadrons incorrectly identified as electrons, and electrons not from heavy-flavor hadron decays. To estimate the contribution of the hadron contamination in the trigger-electron sample, a sample of identified hadrons is obtained by applying a selection of $n\sigma_e^{\text{TPC}} < -3.5$ on the reconstructed tracks. The corresponding E/p distribution from these hadrons is normalized by the electron-candidate E/p in the region $0.25 < E/p < 0.5$, which is displaced sufficiently from the electron peak, in order to match the hadron contamination in the electron-candidate E/p distribution. The normalized hadron E/p is subtracted from the electron-candidate E/p distribution to obtain the hadron-contamination corrected E/p distribution. The number of hadrons from the normalized hadron distribution in the region of $0.8 < E/p < 1.2$ reflects the contamination ($N_{\text{had,contam.}}$) in the electron-candidate sample. This procedure follows a method similar to that described in Refs. [11, 77]. The average contamination is 5% (2.5%) at $p_T^e = 4 \text{ GeV}/c$ in the 0–10% (30–50%) centrality interval, and 22% (18%) at $p_T^e = 16 \text{ GeV}/c$

in the 0–10% (30–50%) centrality interval. To remove the hadron contamination in the $\Delta\phi$ correlation distribution, an additional distribution is obtained by selecting trigger particles with $n\sigma_e^{\text{TPC}} < -3.5$. This hadron-triggered correlation distribution is normalized by $N_{\text{had,contam.}}$ and subtracted from the electron-candidate correlation distribution to obtain the hadron-contamination corrected $\Delta\phi$ distribution. The electron sample after hadron contamination removal will be referred to as inclusive electrons (Incl.e).

The resulting azimuthal-correlation distributions also contain a background contribution from electrons not originating from heavy-flavor hadrons. The signal electron sample for this analysis originates from heavy-flavor hadron semileptonic decays, which produce a single electron. The primary sources of the background electrons in the p_T^e regions studied are Dalitz decays of neutral mesons ($\pi^0 \rightarrow \gamma e^+ e^-$ and $\eta \rightarrow \gamma e^+ e^-$) and photon conversions ($\gamma \rightarrow e^+ e^-$) within the detector material. The electrons resulting from these background sources originate from electron-positron pairs with a small value of invariant mass. To identify these background electrons, unlike-sign (ULS) pairs are built and their invariant mass ($m_{e^+e^-}$) is reconstructed using a technique described in Refs. [73, 78], resulting in a signal peak from the photon conversions and Dalitz decays. Partner electrons are selected using similar but looser track-quality and electron-identification criteria than those applied to the trigger tracks, in order to optimize the efficiency of reconstructing the partner (Refs. [43, 78]). Trigger electrons are paired with a partner electron identified with the TPC selection $-3 < n\sigma_e^{\text{TPC}} < 3$ to maximize the selection efficiency. The invariant-mass distribution of combinatorial electron pairs is estimated by reconstructing like-sign electron (LS) pairs. Unlike in the equivalent analysis in pp and p–Pb collisions [11], the background of the LS invariant-mass distribution in Pb–Pb collisions does not perfectly match with the ULS distribution, likely due to detector effects. For $4 < p_T^e < 12 \text{ GeV}/c$, the LS distribution is thus scaled by a normalization factor of 1.045 to match the ULS distribution in the invariant-mass region $0.2 < m_{e^+e^-} < 0.25 \text{ GeV}/c^2$, a region which is sufficiently displaced from the signal peak. The corresponding scale factors for trigger ranges $4 < p_T^e < 7$ and $7 < p_T^e < 16 \text{ GeV}/c$ are 1.038 and 1.114, respectively. Electrons matched with ULS and LS partners are used to construct azimuthal-correlation distributions, $S(\Delta\phi)^{\text{ULS}}$ and $S(\Delta\phi)^{\text{LS}}$, respectively. Background contributions are removed by subtracting the LS distribution from the ULS distribution, considering only electron pairs with $m_{e^+e^-} < 0.14 \text{ GeV}/c^2$, which captures the majority of the signal from photon conversions and Dalitz decays. The resulting distribution, $(S(\Delta\phi)^{\text{ULS}} - S(\Delta\phi)^{\text{LS}})$, is then corrected for the partner-finding efficiency, referred to as the tagging efficiency (ϵ_{tag}), which is estimated from Monte Carlo simulations following a similar procedure as in Refs. [78, 79]. The resulting correlation distribution between electrons from heavy-flavor hadron decays and charged particles, $(S(\Delta\phi)^{\text{c,b}\rightarrow e})$, is calculated as

$$S(\Delta\phi)^{\text{c,b}\rightarrow e} = S(\Delta\phi)^{\text{Incl.e}} - \frac{1}{\epsilon_{\text{tag}}} [S(\Delta\phi)^{\text{ULS}} - S(\Delta\phi)^{\text{LS}}]. \quad (2)$$

The Monte Carlo sample used for determining the tagging efficiency is obtained using HIJING v1.36 [80], from now on referred to as HIJING. The particle propagation through the ALICE apparatus is simulated using GEANT3 [81]. To improve the statistical precision of the tagging efficiency, additional π^0 and η mesons generated with PYTHIA 6.4.25 [82] are embedded into the simulated sample, extending their spectra to a high- p_T range. For collisions in the 0–10% (30–50%) centrality interval, the tagging efficiency is $57 \pm 1\%$ ($61 \pm 1\%$) at $p_T^e = 4 \text{ GeV}/c$, and approximately $65 \pm 1\%$ ($68 \pm 1\%$) at $p_T^e = 7 \text{ GeV}/c$. For $p_T^e > 8 \text{ GeV}/c$, the tagging efficiency is approximately constant with a value of $70 \pm 1\%$ for both centrality classes. Other sources of electrons, such as from J/ψ , kaon, and light vector meson (ρ , ω , and ϕ) decays, are negligible in the p_T^e ranges used in this analysis [83].

The $S(\Delta\phi)^{\text{c,b}\rightarrow e}$ distribution is corrected for detector inefficiencies in reconstructing associated particles and for contamination from secondary particles within the associated-particle sample. The associated-particle reconstruction efficiency for charged primary particles is obtained from simulated Pb–Pb collisions produced with the HIJING [80] event generator. In the interval $1 < p_T^{\text{assoc.}} < 7 \text{ GeV}/c$, for 0–10%

(30–50%) collisions, the efficiency is 82–85% (86–87%). This simulated sample is also used to estimate the contamination of secondary particles in the associated-particle sample. The secondary contamination is 2–4% (1–4%) for 0–10% (30–50%) collisions. The efficiency for trigger-electron reconstruction and selection is approximately constant within the measurement interval, so no correction is needed. The resulting azimuthal-correlation distribution is normalized by the number of trigger electrons from heavy-flavor hadron decays ($N_{c,b \rightarrow e}$), which is obtained from the number of inclusive electrons ($N_{\text{Incl},e}$) and the number of electrons ULS and LS pairs using

$$N_{c,b \rightarrow e} = N_{\text{Incl},e} - \frac{1}{\epsilon_{\text{tag}}} (N_{\text{ULS}} - N_{\text{LS}}). \quad (3)$$

3.4 Baseline estimation and fit function for the azimuthal-correlation distributions

In the high-multiplicity environment of Pb–Pb collisions, the per-trigger normalized azimuthal-correlation distribution is affected by a significant background contribution from particle pairs not originating from the same hard scattering process. While this background is typically flat in $\Delta\varphi$ and lies beneath the physically correlated peaks, the presence of collective motion in the medium introduces an additional modulation due to the anisotropic flow of electrons from heavy-flavor hadron decays and the flow of associated charged particles. In this situation, this contribution can be estimated by a baseline function, which is discussed in Ref. [84] and defined as

$$B(\Delta\varphi) = b(1 + 2 \sum_n v_n^{\text{c,b} \rightarrow e} v_n^{\text{assoc}} \cos(n\Delta\varphi)), \quad (4)$$

where $v_n^{\text{c,b} \rightarrow e}$ and v_n^{assoc} are the n-th order harmonic flow coefficients of electrons from heavy-flavor hadron decays and charged associated particles, respectively. For this study, only the v_2 and v_3 flow coefficients are considered and the higher-order flow coefficients (for $n \geq 4$), accounting for a negligible contribution to $B(\Delta\varphi)$, are neglected. Measurements by the ATLAS experiment of the second and third flow coefficients for muons produced from heavy-flavor hadron decays at midrapidity in Pb–Pb collisions at $\sqrt{s_{\text{NN}}} = 5.02$ TeV in the 0–10% and 30–40% centrality classes [85] are used for the $v_2^{\text{c,b} \rightarrow e}$ and $v_3^{\text{c,b} \rightarrow e}$ parameters. The ATLAS $v_n^{\text{c,b} \rightarrow \mu}$ is used in place of $v_n^{\text{c,b} \rightarrow e}$ values due to the lack of measurements of inclusive electrons from heavy-flavor hadron decays in the p_T and centrality intervals of this analysis. Flow coefficients of charged particles $v_2^{\text{ch. part.}}$ and $v_3^{\text{ch. part.}}$ measured in different Pb–Pb centrality intervals [86] at midrapidity are utilized for v_n^{assoc} . The measured p_T spectra of muons from heavy-flavor hadron decays [49] and charged particles [87] are used to compute a statistically weighted average of the v_n values within the p_T ranges relevant to this analysis.

The von Mises distribution approximates the circular analogue of the normal distribution and is used in directional statistics to model the distribution of periodic data [88]. For this reason, it is employed in similar analyses of pp and p–Pb collisions to characterize the NS and AS peaks [11]. The following fit function is applied to the fully-corrected per-trigger correlation distribution,

$$f(\Delta\varphi) = B(\Delta\varphi) + \frac{A e^{\kappa_{\text{NS}} \cos(\Delta\varphi)}}{2\pi I_0(\kappa_{\text{NS}})}. \quad (5)$$

Equation 5 is composed of a von Mises function to describe the NS peak, combined with the baseline function $B(\Delta\varphi)$ from Eq. 4, which accounts for the uncorrelated background and flow contributions. For the von Mises function, the mean is fixed at $\Delta\varphi = 0$ to characterize the NS peak. The v_n values in $B(\Delta\varphi)$ are fixed, while the other parameters are left free. The κ_{NS} term quantifies the concentration of the NS peak, where $1/\kappa_{\text{NS}}$ corresponds to the variance σ^2 for a circular distribution. I_0 denotes the zeroth-order modified Bessel function evaluated at κ_{NS} , and A represents the integral of the NS peak.

For some p_T^{assoc} intervals in both centrality classes, no AS peak is observed. When an AS peak is evident, its shape is not consistently described by a Gaussian distribution. Due to this p_T -dependent behavior and to ensure a stable fit for determining the baseline position, the correlation distribution is fitted with Eq. 5 in the transverse region and the NS peak region, excluding the AS peak range $1.96 < \Delta\phi < 4.3$ rad. The baseline function position is then determined from this fit procedure for all p_T^{assoc} intervals. After subtracting the baseline, the per-trigger yields are obtained by integrating the distribution within the NS and AS peak regions in $\Delta\phi$, as detailed in Sec. 5.

4 Systematic uncertainties

The $\Delta\phi$ correlation distribution and the resulting NS and AS per-trigger yield observables are subject to systematic uncertainties related to the analysis procedure. These uncertainties originate from the electron-track selection process, electron identification and subtraction of the hadron contamination, the background-electron subtraction, the associated-particle efficiency correction, the mixed-event correction procedure, and the baseline estimation on the correlation distribution. Each of these uncertainty sources is estimated separately by varying the selection criteria or by introducing an alternative approach to estimate a specific quantity. The systematic uncertainty is evaluated by examining the ratio of the correlation distribution or the per-trigger yield obtained from each variation to that from the nominal configuration. The systematic uncertainties on the correlation distribution from the associated-particle efficiency and the mixed-event correction are considered correlated since their source contribution varies by the same amount within $\Delta\phi$, while all other sources are considered uncorrelated due to the uncertainty varying as a function of $\Delta\phi$.

The evaluation of each systematic uncertainty is performed separately for each trigger- and associated- p_T interval, and for each centrality interval. A summary of the systematic uncertainties affecting the correlation distribution, the NS and the AS peaks, for $4 < p_T^e < 12$ GeV/ c , are reported in Tables 1 and 2 for the 0–10% and 30–50% centrality classes. Correlated and uncorrelated uncertainties in $\Delta\phi$ are separated in Table 1. The total uncertainty is reported for the per-trigger peak yields in this table. Table 2 reports the baseline pedestal value (b) obtained from the nominal baseline determination method (Eq. 5) for each p_T^{assoc} interval, along with the corresponding absolute systematic uncertainties estimated from variations in the baseline determination. The NS and AS peak yields and their absolute systematic uncertainties arising solely from baseline estimation, are reported for both centrality classes in this table.

Table 1: Systematic uncertainties from various sources (excluding baseline estimation) on the azimuthal-correlation distribution, as well as NS and AS peak yields, are reported for $4 < p_T^e < 12$ GeV/ c in 0–10% (30–50%) central Pb–Pb collisions. Total uncertainties from $\Delta\phi$ -correlated and uncorrelated sources on the correlation distribution are provided separately.

Source	$\Delta\phi$ distribution	NS yield	AS yield
Electron-track selection	5% (2%)	5% (2%)	5% (3%)
Electron identification	3% (1%)	3% (2%)	4% (2%)
Background electron	5% (3%)	5% (3%)	5% (4%)
Associated particle selection	5% (3%)	5% (3%)	5% (3%)
Mixed-event correction	2% (2%)	2% (2%)	2% (2%)
Total (correlated sources)	5.4% (3.6%)		
Total (uncorrelated sources)	< 7.7% (< 3.7%)		
Total		9.4% (7.1%)	9.7% (7.6%)

To estimate the uncertainty due to potential biases introduced by the electron-candidate track-quality selection, the same type of quality selection criteria to what is reported in Ref. [73] are varied, in particular,

Table 2: Estimate of the pedestal value (b) of the azimuthal-correlation distributions together with its absolute systematic uncertainty in the interval $4 < p_T^e < 12 \text{ GeV}/c$ in Pb–Pb collisions in the 0–10% and 30–50% centrality classes. The NS and AS associated peak yields are also reported together the absolute systematic uncertainty due to the baseline estimation.

$p_T^{\text{assoc}} (\text{GeV}/c)$	$b (\text{rad}^{-1})$	NS yield	AS yield
0–10% centrality class			
1 – 2	103.0 ± 0.065	0.953 ± 0.154	0.765 ± 0.206
2 – 3	15.37 ± 0.025	0.412 ± 0.039	0.155 ± 0.078
3 – 4	2.429 ± 0.010	0.134 ± 0.016	0.035 ± 0.033
4 – 5	0.357 ± 0.003	0.042 ± 0.004	0.010 ± 0.010
5 – 7	0.061 ± 0.002	0.027 ± 0.002	0.005 ± 0.005
30–50% centrality class			
1 – 2	24.28 ± 0.037	0.608 ± 0.087	0.006 ± 0.115
2 – 3	3.756 ± 0.014	0.277 ± 0.022	0.162 ± 0.043
3 – 4	0.685 ± 0.006	0.116 ± 0.009	0.023 ± 0.018
4 – 5	0.118 ± 0.003	0.042 ± 0.003	0.018 ± 0.008
5 – 7	0.023 ± 0.001	0.027 ± 0.002	0.017 ± 0.004

requirements on the number of crossed TPC pad rows, the number of crossed rows over findable clusters. The number of crossed rows requirement is varied by ± 10 from the nominal value, and the number of crossed rows over findable clusters is varied by ± 0.1 from the nominal value. For the 0–10% (30–50%) centrality interval, there is an estimated 5% (2%) uncertainty on the correlation distribution in the trigger interval of $4 < p_T^e < 12 \text{ GeV}/c$. The systematic uncertainty for the electron-track selection is estimated to be within 5% (2%) for the NS peak yields, and 5% (3%) for the AS peak yields in the 0–10% (30–50%) centrality classes.

The uncertainty on the estimation of the hadron contamination affecting the purity of the electron sample, and on the stability of the electron-identification criteria, and their impact on the correlation distribution is estimated by varying the identification criteria on the TPC and EMCAL signals, i.e., of $n\sigma_e^{\text{TPC}}$, E/p , and σ_{long}^2 . A full background subtraction procedure is performed for each variation. The variations in the selection criteria result in a change of electron purity and efficiency of 3% and 10%, respectively. The total uncertainty determined from these sources is 3% (1%) for the $\Delta\phi$ distribution, 3% (2%) for the NS peak yields, and 4% (2%) for the AS peak yields in the 0–10% (30–50%) centrality class.

The background-electron contribution from photon conversion and Dalitz decays is estimated via the invariant-mass method. A systematic uncertainty estimation on such a correction is performed by varying the selection of the partner electron tracks, such as the minimum p_T of the partner electron ($\pm 0.1 \text{ GeV}/c$ from the nominal value of $0.3 \text{ GeV}/c$, the track-quality selection [73], and the invariant-mass threshold of the electron-positron pairs ($10 \text{ MeV}/c^2$ around the nominal value of $140 \text{ MeV}/c^2$). These variations primarily affect the tagging efficiency, which varies by 20% (17%) in the 0–10% (30–50%) centrality class. The systematic uncertainty is 5% (3%) for the $\Delta\phi$ distribution, 5% (3%) for the NS peak yields, and 5% (4%) for the AS peak yields, for $4 < p_T^e < 12 \text{ GeV}/c$ in 0–10% (30–50%) centrality class, respectively.

The uncertainty resulting from the track-selection criteria applied to the associated charged particles is estimated by varying the number of TPC crossed pad rows (± 10), the number of crossed rows over findable clusters (± 0.1), and the η requirement (± 0.1) from the nominal value. This uncertainty is considered correlated in $\Delta\phi$. Uncertainty values of 5% (3%) for both the distribution and peak yields are obtained for $4 < p_T^e < 12 \text{ GeV}/c$ interval for the 0–10% (30–50%) centrality class.

To estimate the uncertainty due to the mixed-event correction, the criteria used for normalizing the mixed-event distributions are varied by slightly changing the multiplicity and z -vertex selection pools. As an

additional systematic check, the mixed-event normalization factor β (see Eq. 1) is obtained considering the integrated distribution yield over the full $\Delta\phi$ range for $|\Delta\eta| < 0.01$. A correlated uncertainty of 2% is estimated for the $\Delta\phi$ distribution as well as for the NS and AS peak yields in both centrality classes in the $4 < p_T^e < 12 \text{ GeV}/c$ interval.

The largest source of systematic uncertainty arises from evaluating the baseline function, which depends on the value of b and the uncertainties on the measured v_n values in Eq. 4. Two methods are used to estimate the systematic uncertainty of the baseline pedestal (b) position. First, the fit uncertainty of the b parameter (σ_b) from Eq. 5 is used to define two baseline variations by adjusting the b parameter from its central value to $b \pm \sigma_b$. The second method involves fitting the correlation distribution with the baseline function, Eq. 4, in three transverse regions: $-\pi/2 < \Delta\phi < -1.18 \text{ rad}$ (left), $|\Delta\phi - \pi/2| < 0.4 \text{ rad}$ (middle), and $4.3 < \Delta\phi < 3\pi/2 \text{ rad}$ (right), excluding the NS and AS peak regions. The average b parameter from these three fits is then calculated. Furthermore, the definitions of the transverse regions are varied for additional systematic checks, and the corresponding b parameters are obtained. An additional systematic check is conducted to assess whether the uncertainties in the v_n measurement affects the baseline and peak yields. This is done by varying v_n by $\pm \sigma_{v_n}$, where σ_{v_n} represents the combined statistical and systematic uncertainties of the measured values. It is found that the uncertainty due to σ_{v_n} is negligible compared to the uncertainty on the pedestal b . The overall systematic uncertainty is calculated by taking the difference between the largest and smallest of the considered baseline variations. The uncertainty from the baseline estimation on the correlation distribution is reported as an absolute value, affecting all $\Delta\phi$ bins equally. Unlike other uncertainties in the measurement, the baseline uncertainty does not intrinsically alter the overall correlation distribution but shifts the yield within a given uncertainty. Therefore, when plotting the NS and AS peak yields, the uncertainty from the baseline estimation is presented separately from other sources.

The above systematic estimation procedures are repeated to estimate the systematic uncertainties from the above mentioned sources on the correlation distribution, NS and AS yields for $4 < p_T^e < 7 \text{ GeV}/c$ and $7 < p_T^e < 16 \text{ GeV}/c$. The uncertainty values are found to be similar to those obtained for $4 < p_T^e < 12 \text{ GeV}/c$.

5 Results

The azimuthal-correlation distributions between electrons from heavy-flavor hadron decays and charged particles in 0–10% and 30–50% Pb–Pb collisions at $\sqrt{s_{\text{NN}}} = 5.02 \text{ TeV}$ are presented for different trigger electron and associated charged-particle p_T intervals. The baseline subtracted correlation distributions in Pb–Pb collisions are compared to those from pp collisions. The per-trigger associated yields ($1/N^{(\text{c},\text{b}) \rightarrow e} N^{\text{assoc}}$) on the NS and AS of the correlation distributions are obtained and are also compared to those in pp collisions. The per-trigger yields from the two collision systems are used to calculate the per-trigger nuclear modification factor (I_{AA}). The I_{AA} is defined as the ratio of the per-trigger yield in Pb–Pb ($Y_{\Delta\phi}^{\text{Pb–Pb}}$) over the per-trigger yield in pp ($Y_{\Delta\phi}^{\text{pp}}$) [7, 8, 53],

$$I_{\text{AA}} = \frac{Y_{\Delta\phi}^{\text{Pb–Pb}}}{Y_{\Delta\phi}^{\text{pp}}}, \quad (6)$$

obtained in the $\Delta\phi$ interval corresponding to the correlation peak for Pb–Pb and pp, respectively. The resulting I_{AA} are compared to those measured from correlations triggered by inclusive charged hadrons and K_S^0 mesons to study the flavor dependence of the modification of the associated-particle yields.

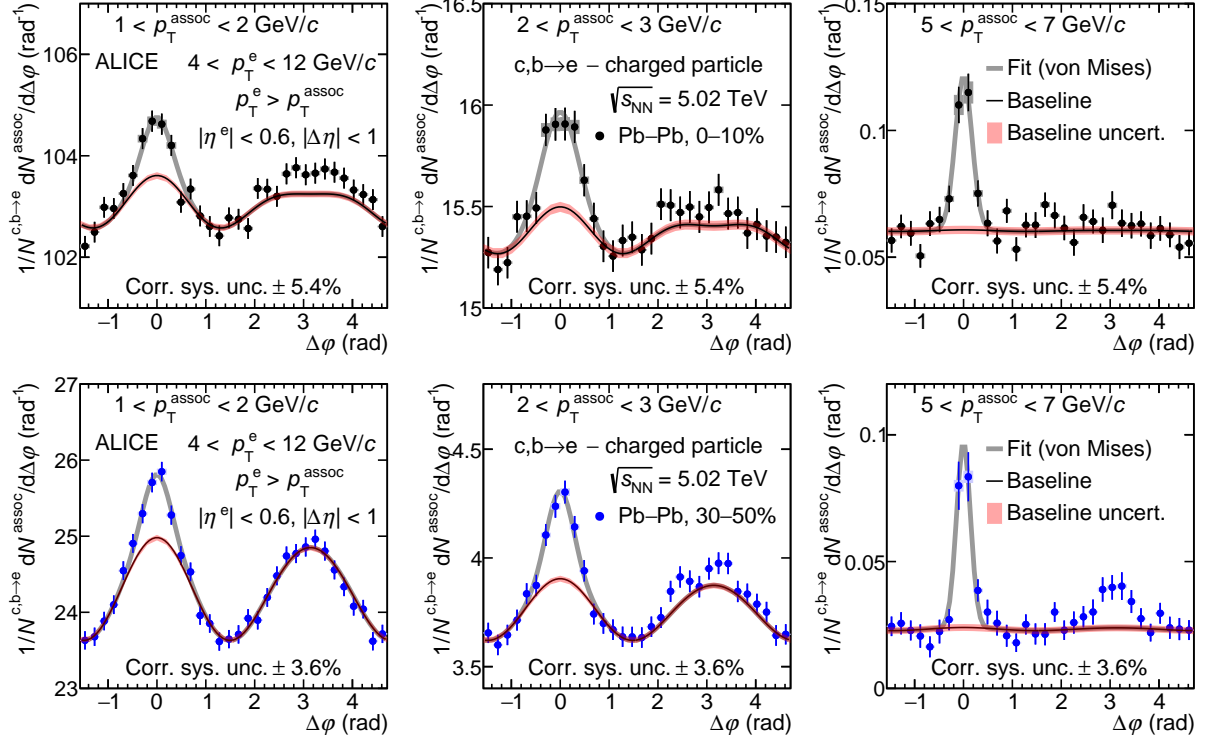


Figure 1: Azimuthal-correlation distributions of electrons from heavy-flavor hadron decays and charged particles before baseline subtraction for $4 < p_T^e < 12 \text{ GeV}/c$ and different associated p_T intervals, for the central (0–10%, top panels) and semicentral (30–50%, bottom panels) Pb–Pb collisions at $\sqrt{s_{\text{NN}}} = 5.02 \text{ TeV}$. The distributions are fitted with a von Mises function to describe the NS peak (solid gray line) and a baseline function which includes a constant term and v_n modulations (solid black curve). The statistical (uncorrelated systematic) uncertainties are shown as vertical lines (filled boxes). The uncertainties on the baseline are shown with a red band.

5.1 $\Delta\phi$ distributions

Figure 1 shows the azimuthal-correlation distributions between trigger electrons in the interval $4 < p_T^e < 12 \text{ GeV}/c$ and associated particles in different p_T intervals, with the fit function defined in Eq. 5, measured in Pb–Pb collisions in 0–10% (top panels) and 30–50% (bottom panels) centrality intervals. The remaining p_T intervals are shown in Appendix A. The correlated systematic uncertainties, from the associated-particle selection and mixed-event correction, are reported in the legend for each p_T^{assoc} interval. The $\Delta\phi$ -correlated uncertainty on the baseline is shown as dotted curves.

The baseline contribution, which depends on the charged-particle multiplicity, is higher in 0–10% central events compared to 30–50% central events, with its value decreasing with increasing p_T^{assoc} in both centrality intervals. A significantly large v_n contribution dominates the AS peak at low p_T^{assoc} . For both collision centrality classes, the NS peak height decreases and its width narrows as p_T^{assoc} increases.

To study the impact of the QGP medium on the NS and AS peaks of the $\Delta\phi$ -correlation distribution, the baseline-subtracted distributions in Pb–Pb collisions for 0–10% and 30–50% centrality classes are compared to those obtained in pp collisions [11]. The comparison is performed for $4 < p_T^e < 12 \text{ GeV}/c$ and for different p_T^{assoc} intervals, as shown in Fig. 2 for the 0–10% centrality class and Fig. 3 for the 30–50% centrality class. The shape of the NS peaks for 0–10% central Pb–Pb collisions follows a similar trend to that of pp collisions within the statistical and systematic uncertainties, such that the peak narrows as a function of p_T^{assoc} . Concurrently, the AS peak tends towards a suppression compared to pp collisions for $p_T^{\text{assoc}} > 3 \text{ GeV}/c$. For Pb–Pb collisions in the 30–50% centrality class, the NS peak

shapes are consistent with those of pp collisions for all p_T^{assoc} . However, the AS peaks in semicentral Pb–Pb collisions tend to be lower than in pp collisions within large statistical uncertainties. The observed modifications on the AS of the $\Delta\varphi$ distributions in Pb–Pb collisions potentially indicate the presence of interactions between the medium and the parton recoiling from the heavy quark, as well as the related shower [7, 57, 89, 90].

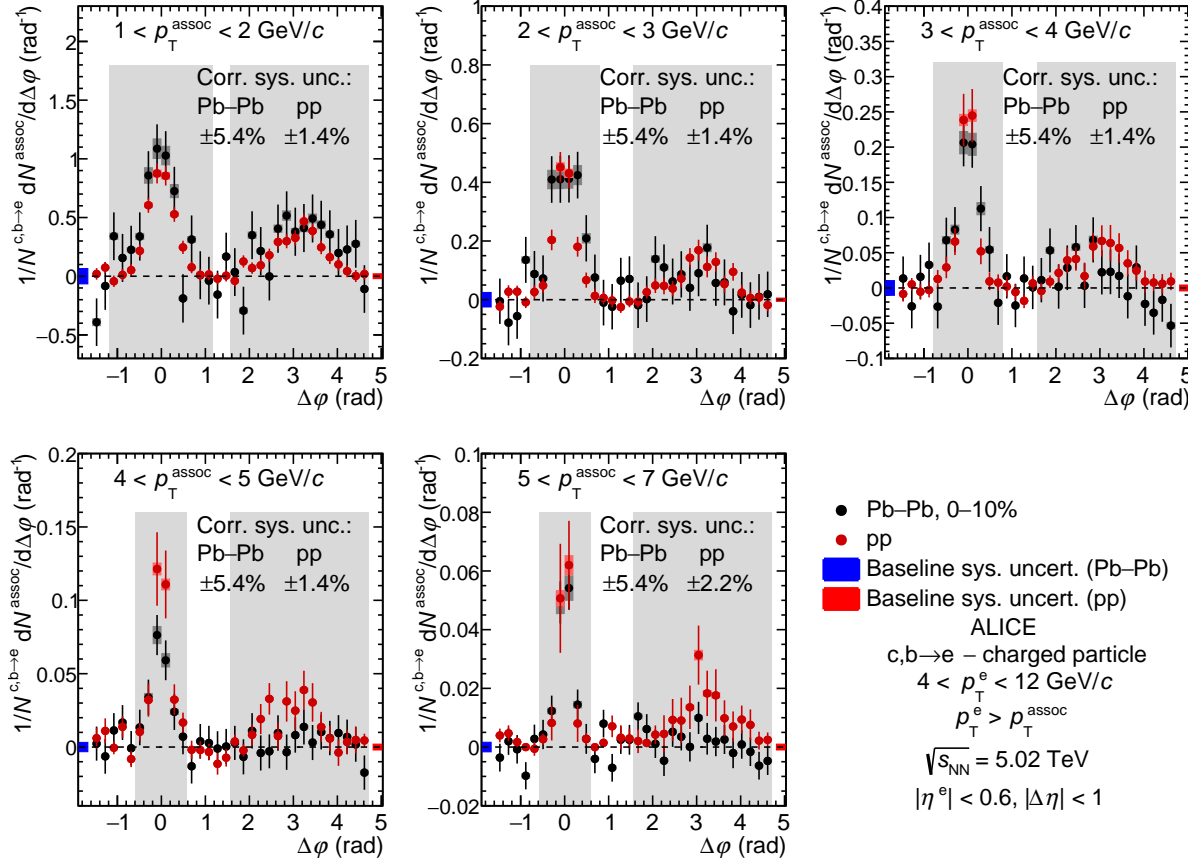


Figure 2: Comparison of the azimuthal-correlation distributions of electrons from heavy-flavor hadron decays and charged particles measured in the 0–10% centrality class Pb–Pb collisions and in pp collisions [11], after the baseline subtraction, for $4 < p_T^e < 12 \text{ GeV}/c$ and different associated p_T intervals. The statistical (uncorrelated systematic) uncertainties are shown as vertical lines (filled boxes). The uncertainties on the baseline estimation are shown as solid boxes at $\Delta\varphi \sim -2$ and 5 rad. The shaded gray area corresponds to the integrated regions in $\Delta\varphi$ to obtain the NS and AS yield.

5.2 Per-trigger associated-particle yield and per-trigger nuclear modification factor

To perform a quantitative comparison of the correlation peaks between pp and Pb–Pb collisions, the per-trigger associated yields on the NS and AS peaks are evaluated as a function of p_T^{assoc} for $4 < p_T^e < 12 \text{ GeV}/c$, as shown in Fig. 4 for both collision centrality classes. The yields are obtained by integrating the baseline-subtracted correlation distributions in the $\pm 3\sigma$ region from the center of the NS and AS peak regions along $\Delta\varphi$, where σ is taken from the pp peak width value estimated from PYTHIA and obtained from the study in Ref. [11]. The σ_{NS} values used in this analysis (as a function of increasing p_T^{assoc}) are: $\sigma_{\text{NS}} = 0.33, 0.25, 0.2, 0.175, 0.15$. Due to the size of the uncertainty in the pp AS width measurement, the AS per-trigger yields were determined by integrating the correlation distribution in a fixed region of $\pm 3\sigma_{\text{AS}}$ (with $\sigma_{\text{AS}} = 0.5$). The integration regions for the peak yields are shown in Fig. 2 and Fig. 3. This integration region is the same for distributions from both Pb–Pb and pp collisions.

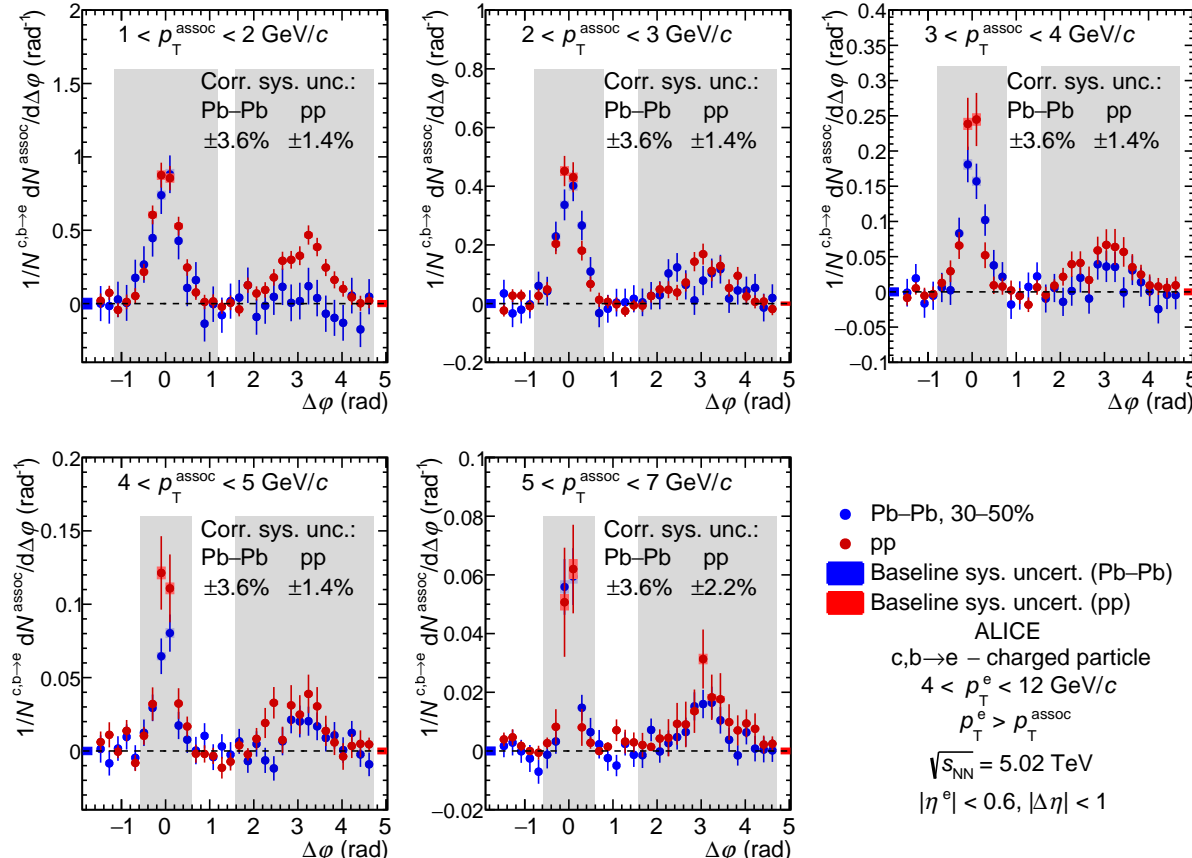


Figure 3: Comparison of the azimuthal-correlation distributions of electrons from heavy-flavor hadron decays and charged particles measured in the 30–50% centrality class Pb–Pb collisions and in pp collisions [11], after the baseline subtraction, for $4 < p_T^e < 12$ GeV/c and different associated p_T intervals. The statistical (uncorrelated systematic) uncertainties are shown as vertical lines (filled boxes). The uncertainties on the baseline estimation are shown as solid boxes at $\Delta\phi \sim -2$ and 5 rad. The shaded gray area corresponds to the integrated regions in $\Delta\phi$ to obtain the NS and AS yield.

The systematic uncertainty on the yield due to the baseline estimation is presented separately (empty box) from other sources (solid box). The AS Pb–Pb yield in several p_T^{assoc} intervals is consistent with zero within one standard deviation, accounting for statistical and systematic uncertainties combined in quadrature. This may be due to a strong suppression from in-medium energy loss. In these intervals, upper limits of the yield value at 68% and 95% confidence levels are evaluated and are represented with arrows. The NS and AS yields are observed to decrease with increasing p_T^{assoc} across pp, p–Pb [11], and Pb–Pb collision systems.

The ratios of the per-trigger associated NS and AS yields in Pb–Pb to pp collisions are calculated in each kinematic interval to obtain the per-trigger nuclear modification factors, I_{AA} . The I_{AA} observable quantifies the effect of the QGP medium, in particular for the NS, on the jet which is directly produced by the fragmentation of a heavy quark and any potential effect of the jet on the medium. The I_{AA} of associated yields on the NS and AS for both collision centrality classes are shown as a function of p_T^{assoc} for $4 < p_T^e < 12$ GeV/c in Fig. 5. For the kinematic intervals showing AS yields consistent with zero within one standard deviation of total uncertainties, the related I_{AA} are also reported as upper limits for 68% and 95% confidence levels, and shown with an arrow. In 0–10% central Pb–Pb collisions, the I_{AA} on the NS side shows a slight hint of an increase at $p_T^{\text{assoc}} < 3$ GeV/c, albeit with a significance of only 1.27σ .

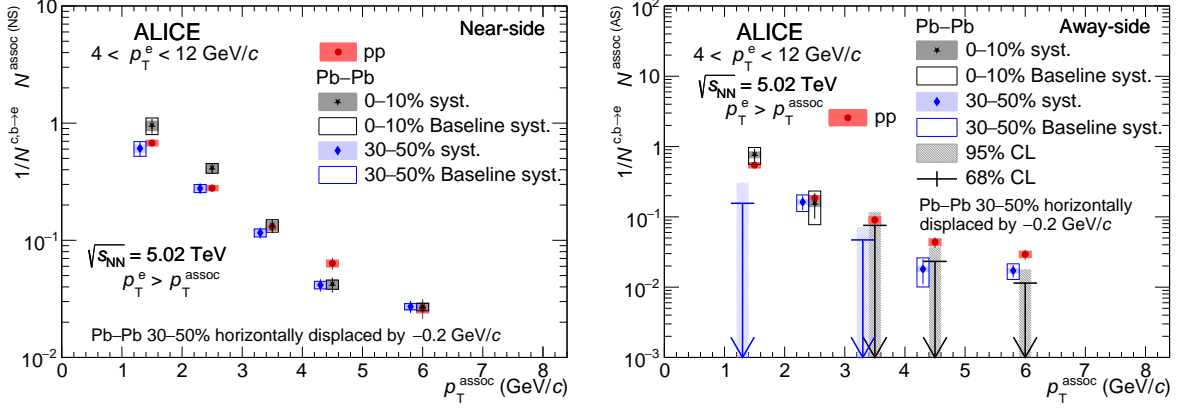


Figure 4: Per-trigger associated yields of the NS (left) and AS (right) peaks for $4 < p_T^e < 12 \text{ GeV}/c$ as a function of p_T^{assoc} in Pb–Pb collision centrality classes 0–10% and 30–50%, compared to those obtained from minimum-bias pp collisions. The statistical (systematic) uncertainties are shown as vertical lines (empty boxes). In some p_T^{assoc} intervals, the AS yield is consistent with zero within one standard deviation of statistical and systematic uncertainties added in quadrature. For those intervals, upper limits on the yields for 68% and 95% confidence levels are evaluated, and are shown with arrows and boxes, respectively.

for $1 < p_T^{\text{assoc}} < 3 \text{ GeV}/c$, considering the statistical, systematic, and baseline uncertainties combined in quadrature. There are multiple possible interplaying mechanisms that would cause an enhancement, such as k_T broadening, medium excitation, or possible fragments from radiated gluons [89, 91–94]. At higher p_T^{assoc} , the I_{AA} is consistent with unity. On the AS, the I_{AA} shows a p_T^{assoc} dependence, with values consistent with unity at low p_T^{assoc} . These values decrease to approximately 0.5 for $p_T^{\text{assoc}} > 4 \text{ GeV}/c$, indicating a suppression in the higher p_T interval, with a significance of 2.5σ below unity for $p_T > 4 \text{ GeV}/c$. In semicentral Pb–Pb collisions, the NS I_{AA} is consistent with unity for all p_T^{assoc} intervals of the measurement while the AS I_{AA} is compatible with unity for $p_T^{\text{assoc}} < 3 \text{ GeV}/c$ and shows values lower than unity for $p_T^{\text{assoc}} > 3 \text{ GeV}/c$, albeit with large uncertainties.

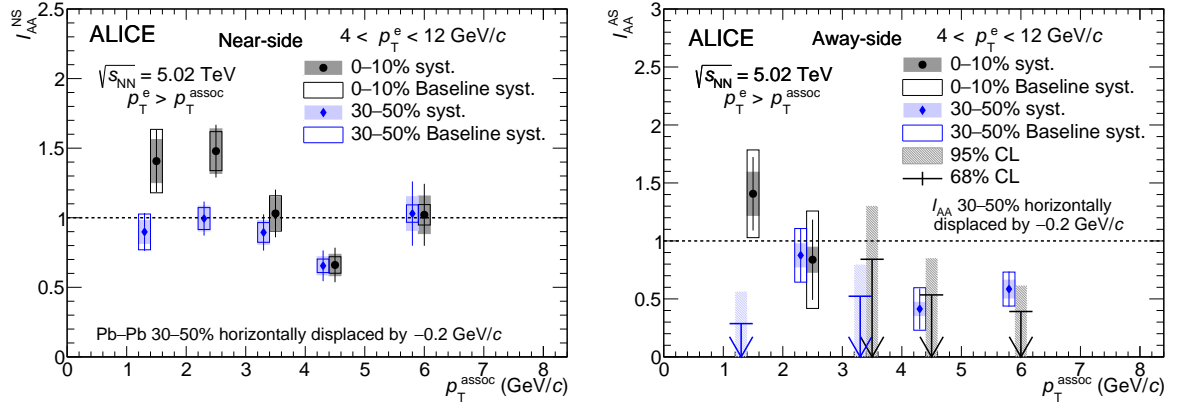


Figure 5: Per-trigger nuclear modification factor (I_{AA}) of NS (left) and AS (right) associated yields, for electrons from heavy-flavor hadron decays in the interval $4 < p_T^e < 12 \text{ GeV}/c$ as a function of p_T^{assoc} in Pb–Pb collisions of centrality classes 0–10% and 30–50%. The statistical (systematic) uncertainties are shown as vertical lines (empty boxes). In some p_T^{assoc} intervals the AS yield is consistent with zero within one standard deviation of total uncertainty. For those intervals, upper limits on the I_{AA} for 68% and 95% confidence levels are shown with arrows and boxes, respectively.

5.3 Dependence of the correlation distributions on the trigger-electron p_T

In pp and p–Pb collisions, the azimuthal-correlation distributions were also measured for two independent trigger electron p_T intervals, $4 < p_T^e < 7 \text{ GeV}/c$ and $7 < p_T^e < 16 \text{ GeV}/c$, to study the dependence on the quark flavor (charm and beauty) from which the trigger electron originates [11]. The fractions of electrons produced by charm- and beauty-hadron decays have a strong p_T dependence, and the beauty contribution is expected to dominate in the higher p_T interval [95, 96]. In pp collisions the electrons from beauty-hadron decays at $p_T^e = 4 \text{ GeV}/c$ account for about 40% of the total electron yield, increasing to 60–70% for $p_T^e > 8 \text{ GeV}/c$. It is observed that the per-trigger associated yield is larger for the higher p_T^e interval, by about 30% at low p_T^{assoc} and by about a factor of 10 in the highest p_T^{assoc} interval, for both pp and p–Pb collisions [11]. By comparing the measurement to PYTHIA Monte Carlo simulations, this behavior is understood to result from heavy quarks of higher energy producing higher- p_T electrons in tandem with a greater number of associated fragmentation particles.

In Pb–Pb collisions, the presence of a QGP induces partonic energy loss, as indicated by the nuclear modification factor (R_{AA}), which depends on the parton momentum and mass. The R_{AA} of electrons from heavy-flavor hadron decays [73] is approximately ~ 0.35 within the p_T^e interval of $4 – 16 \text{ GeV}/c$, with a trend indicating an increasing R_{AA} value towards higher p_T^e . The R_{AA} of particles from beauty-hadron decays is observed to be larger than that of charm hadrons [47–49]. The dependence of the modification of the per-trigger associated-particle production on partonic mass and initial parton energy in the presence of QGP can be studied by measuring the correlation distributions of electrons from heavy-flavor hadron decays and charged particles, and their peak yields for different p_T^e intervals. Figure 6 shows the comparisons of the NS and AS yields for the two p_T^e intervals $4 < p_T^e < 7 \text{ GeV}/c$ and $7 < p_T^e < 16 \text{ GeV}/c$ in 0–10% central Pb–Pb collisions, compared with those obtained for pp collisions. The per-trigger NS and AS yields are systematically higher for the $7 < p_T^e < 16 \text{ GeV}/c$ interval compared to the values obtained for $4 < p_T^e < 7 \text{ GeV}/c$, similar to the observations in pp and p–Pb collisions [11]. This is expected in Pb–Pb collisions as well, as more energetic heavy quarks produce higher- p_T electrons and a greater number of accompanying particles from the quark fragmentation.

Figure 7 shows the corresponding per-trigger nuclear modification factors I_{AA} for the two p_T^e intervals. The I_{AA} values for the two p_T^e intervals are consistent within statistical and systematic uncertainties on both the NS and AS. This indicates that, within the current uncertainties, the modification of the parton shower producing the associated-particle yield does not significantly depend on the energy and mass of the jet-initiating parton.

5.4 Comparison of the per-trigger nuclear modification factor to that of light-flavor trigger particles

The comparison of the R_{AA} of light-flavor, charm, and beauty hadrons shows a mass-dependent ordering in the low- and intermediate- p_T regions [47, 97]. Pions have the lowest R_{AA} , followed by charm hadrons, with beauty hadrons exhibiting the largest R_{AA} values. This indicates a mass-dependent partonic interaction in the QGP. Comparing the I_{AA} of the correlation peak yields from trigger particles with different light-flavor quark content provides insight into the initiating-parton mass and color-charge dependence of the QGP-induced modification of associated-particle yields.

The NS and AS I_{AA} of associated peak yields from angular-correlation distributions of electrons from heavy-flavor hadron decays and charged hadrons are compared with those of dihadron [53], and K_S^0 charged-hadron correlations [53], as shown in Fig. 8. The trigger p_T intervals used for the comparison are $7 < p_T^e < 16 \text{ GeV}/c$ for electrons (where electrons from beauty-hadron decays dominate), $8 < p_T^{\text{trig}} < 16 \text{ GeV}/c$ for dihadron (with a large component of charged hadrons being pions) and K_S^0 -hadron correlations. The I_{AA} of dihadron and K_S^0 charged-hadron correlations shows an enhancement of low- p_T associated particles on the NS, and I_{AA} consistent with unity observed for high- p_T associated

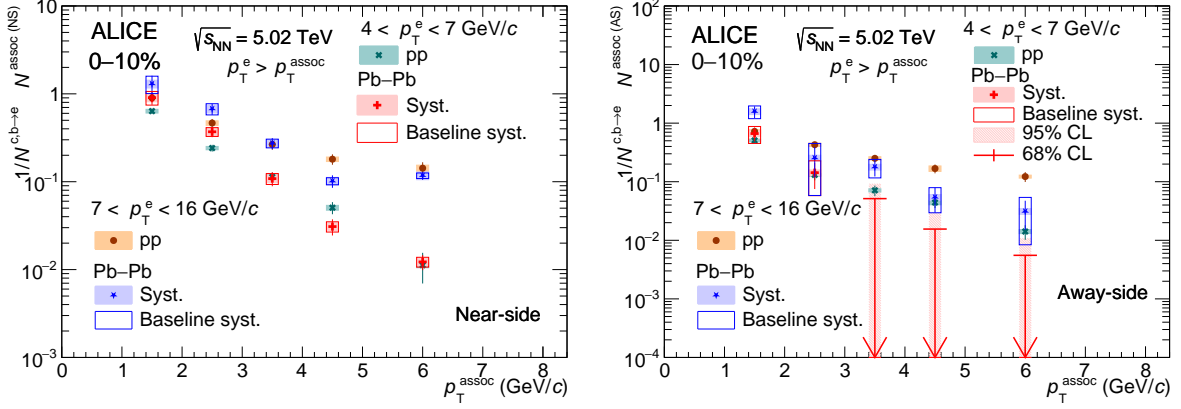


Figure 6: Per-trigger NS (left) and AS (right) associated peak yields for electrons from heavy-flavor hadron decays in the intervals $4 < p_T^e < 7 \text{ GeV}/c$ and $7 < p_T^e < 16 \text{ GeV}/c$ as a function of p_T^{assoc} in central Pb–Pb collisions, compared to measurements in pp collisions [11]. The statistical (systematic) uncertainties are shown as vertical lines (empty boxes). In some p_T^{assoc} intervals the AS yield is consistent with zero within one standard deviation of total uncertainty. For those intervals, upper limits on the yields for 68% and 95% confidence levels are shown with arrows and boxes, respectively.

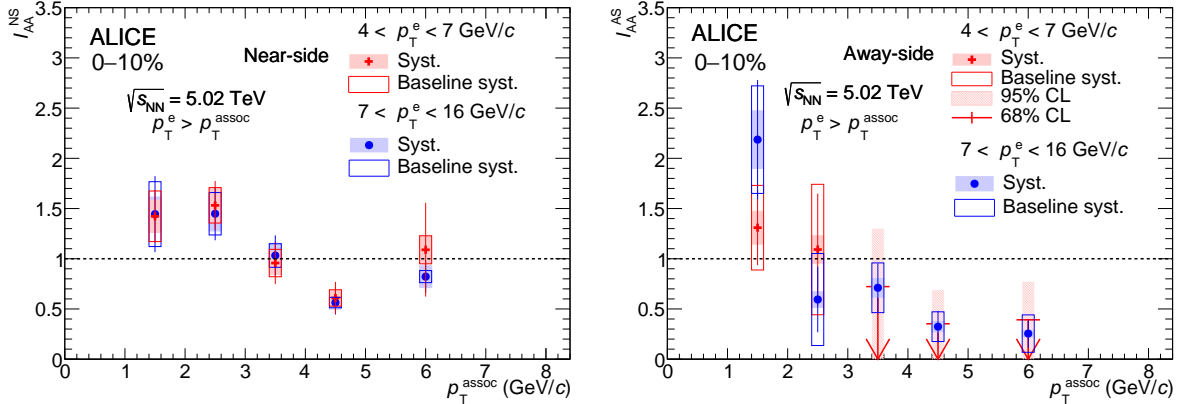


Figure 7: Per-trigger nuclear modification factor (I_{AA}) of the NS (left) and AS (right) associated peak yields for electrons from heavy-flavor hadron decays in intervals $4 < p_T^e < 7 \text{ GeV}/c$ compared to $7 < p_T^e < 16 \text{ GeV}/c$ as a function of p_T^{assoc} in central Pb–Pb collisions. The statistical (systematic) uncertainties are shown as vertical lines (empty boxes). In some p_T^{assoc} intervals the AS yield is consistent with zero within one standard deviation of total uncertainty. For those intervals, upper limits on the I_{AA} for 68% and 95% confidence levels are shown with arrows and boxes, respectively.

particles. On the AS, the associated charged-hadron yield in Pb–Pb collisions is suppressed relative to pp collisions at $p_T^{\text{assoc}} > 4 \text{ GeV}/c$, but an enhancement increasing with decreasing transverse momentum is observed at low p_T^{assoc} [53]. The I_{AA} values of NS and AS yields for electron triggers from heavy-flavor hadron decays are consistent given the current uncertainties with those for light-flavor and strange-particle triggers, indicating no mass dependence on the modification of the associated yield. However, it should be noted that the hadron-to-parton- p_T scaling differs between heavy-flavor and light-flavor quarks; thus, the corresponding parton p_T intervals may not be the same. Additionally, the kinematic differences between the electrons from heavy-flavor hadron decays and K_S^0 or charged hadrons – arising from the decay kinematics of heavy-flavor hadrons – should also be taken into account, along with the additional tracks from these decays that contribute to the NS peak.

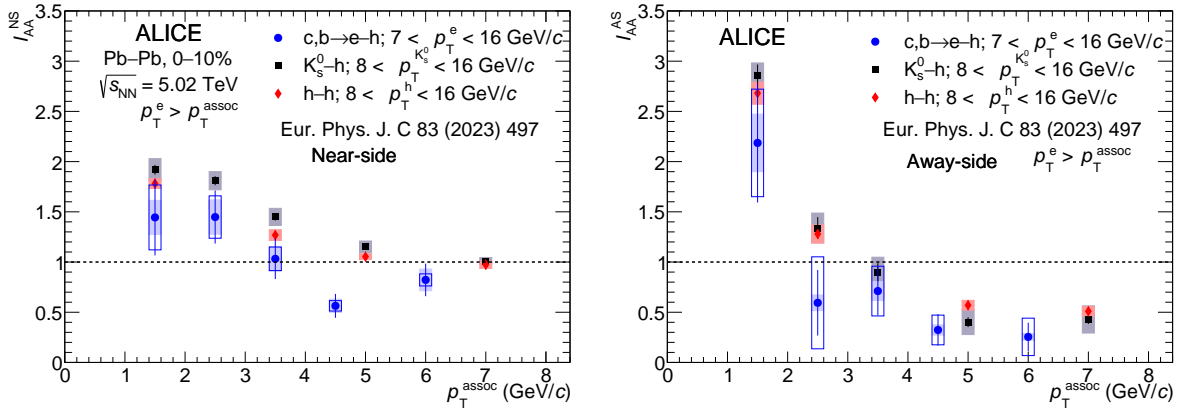


Figure 8: I_{AA} of NS (left) and AS (right) associated peak yield from correlation distributions of electron from heavy-flavor hadron decays as the trigger particle ($7 < p_T^e < 16 \text{ GeV}/c$) compared with that of charged hadrons and K_S^0 as trigger particles ($8 < p_T^{\text{trig}} < 16 \text{ GeV}/c$ [53]).

6 Summary

Azimuthal correlations between electrons from heavy-flavor hadron decays and charged particles in Pb–Pb collisions at $\sqrt{s_{NN}} = 5.02 \text{ TeV}$ are measured for the 0–10% and 30–50% centrality classes. Correlation distributions are obtained for trigger electrons with $4 < p_T^e < 12 \text{ GeV}/c$ and associated charged particles in several p_T intervals from 1 to 7 GeV/c . The results are compared to pp collisions [11], and the per-trigger near-side (NS) and away-side (AS) peak yields are used to compute the per-trigger nuclear modification factor (I_{AA}), which can provide insight into heavy-quark transport in the QGP.

In 0–10% central collisions, the NS I_{AA} suggests a possible enhancement at low p_T^{assoc} , though with limited significance (1.27σ), possibly indicating medium excitation or additional gluon radiation by the propagating high- p_T parton in the QGP. At $p_T^{\text{assoc}} > 3 \text{ GeV}/c$, the NS I_{AA} is consistent with unity. The AS peak I_{AA} is consistent with unity at low p_T^{assoc} but shows a suppression with a 2.5σ significance at higher p_T^{assoc} , likely due to jet energy loss and medium-induced parton shower modifications.

The per-trigger yields are obtained for trigger electrons in $4 < p_T^e < 7 \text{ GeV}/c$ and $7 < p_T^e < 16 \text{ GeV}/c$ in 0–10% central collisions in order to investigate the parton mass and jet-energy dependence. Similar to pp results, trigger electrons with larger p_T^e yield more associated particles in all the p_T^{assoc} intervals of the measurement in both the NS and AS peaks. The NS and AS I_{AA} values remain consistent in both p_T^e intervals within the current uncertainties, suggesting limited dependence on jet energy and initiating parton mass in this kinematic regime.

The I_{AA} for $7 < p_T^e < 16 \text{ GeV}/c$ is also compared to dihadron and K_S^0 correlations [53]. The I_{AA} of electrons from heavy-flavor hadron decays is consistent within uncertainty to the dihadron and K_S^0 I_{AA} at low p_T^{assoc} ($< 3 \text{ GeV}/c$), suggesting an enhancement. All measurements show an AS suppression at high p_T^{assoc} ($> 4 \text{ GeV}/c$). The consistency of I_{AA} across different triggers suggests no clear quark mass dependence given the uncertainties, though variations in hadron-to-parton p_T scales and the additional decay step for the electron from heavy-flavor hadrons could introduce kinematic effects.

These results indicate medium-induced modifications to heavy-flavor jet fragmentation in Pb–Pb collisions, with indications of an increased yield of low- p_T associated particles on the near-side compared to pp collisions. The away-side suppression of high- p_T particles indicates parton energy loss from the recoiling jet to the heavy-flavor jet. Theoretical modeling could further clarify the mechanisms governing heavy-quark propagation in the QGP. During the LHC Run 3, the upgraded ALICE detector [98] is estimated to collect more than an order of magnitude larger Pb–Pb data samples compared to Run 2, which is expected to reduce uncertainties. This will also allow correlation measurements with D mesons

and other charm hadron triggers, which will enable a more precise understanding of the heavy-flavor jet-medium interaction in high-energy heavy-ion collisions.

Acknowledgements

The ALICE Collaboration would like to thank all its engineers and technicians for their invaluable contributions to the construction of the experiment and the CERN accelerator teams for the outstanding performance of the LHC complex. The ALICE Collaboration gratefully acknowledges the resources and support provided by all Grid centres and the Worldwide LHC Computing Grid (WLCG) collaboration. The ALICE Collaboration acknowledges the following funding agencies for their support in building and running the ALICE detector: A. I. Alikhanyan National Science Laboratory (Yerevan Physics Institute) Foundation (ANSL), State Committee of Science and World Federation of Scientists (WFS), Armenia; Austrian Academy of Sciences, Austrian Science Fund (FWF): [M 2467-N36] and Nationalstiftung für Forschung, Technologie und Entwicklung, Austria; Ministry of Communications and High Technologies, National Nuclear Research Center, Azerbaijan; Rede Nacional de Física de Altas Energias (Renafae), Financiadora de Estudos e Projetos (Finep), Fundação de Amparo à Pesquisa do Estado de São Paulo (FAPESP) and The Sao Paulo Research Foundation (FAPESP), Brazil; Bulgarian Ministry of Education and Science, within the National Roadmap for Research Infrastructures 2020-2027 (object CERN), Bulgaria; Ministry of Education of China (MOEC) , Ministry of Science & Technology of China (MSTC) and National Natural Science Foundation of China (NSFC), China; Ministry of Science and Education and Croatian Science Foundation, Croatia; Centro de Aplicaciones Tecnológicas y Desarrollo Nuclear (CEADEN), Cubaenergía, Cuba; Ministry of Education, Youth and Sports of the Czech Republic, Czech Republic; The Danish Council for Independent Research | Natural Sciences, the VILLUM FONDEN and Danish National Research Foundation (DNRF), Denmark; Helsinki Institute of Physics (HIP), Finland; Commissariat à l’Energie Atomique (CEA) and Institut National de Physique Nucléaire et de Physique des Particules (IN2P3) and Centre National de la Recherche Scientifique (CNRS), France; Bundesministerium für Bildung und Forschung (BMBF) and GSI Helmholtzzentrum für Schwerionenforschung GmbH, Germany; General Secretariat for Research and Technology, Ministry of Education, Research and Religions, Greece; National Research, Development and Innovation Office, Hungary; Department of Atomic Energy Government of India (DAE), Department of Science and Technology, Government of India (DST), University Grants Commission, Government of India (UGC) and Council of Scientific and Industrial Research (CSIR), India; National Research and Innovation Agency - BRIN, Indonesia; Istituto Nazionale di Fisica Nucleare (INFN), Italy; Japanese Ministry of Education, Culture, Sports, Science and Technology (MEXT) and Japan Society for the Promotion of Science (JSPS) KAKENHI, Japan; Consejo Nacional de Ciencia (CONACYT) y Tecnología, through Fondo de Cooperación Internacional en Ciencia y Tecnología (FONCICYT) and Dirección General de Asuntos del Personal Académico (DGAPA), Mexico; Nederlandse Organisatie voor Wetenschappelijk Onderzoek (NWO), Netherlands; The Research Council of Norway, Norway; Pontificia Universidad Católica del Perú, Peru; Ministry of Science and Higher Education, National Science Centre and WUT ID-UB, Poland; Korea Institute of Science and Technology Information and National Research Foundation of Korea (NRF), Republic of Korea; Ministry of Education and Scientific Research, Institute of Atomic Physics, Ministry of Research and Innovation and Institute of Atomic Physics and Universitatea Nationala de Stiinta si Tehnologie Politehnica Bucuresti, Romania; Ministerstvo skolstva, vyskumu, vyvoja a mladeze SR, Slovakia; National Research Foundation of South Africa, South Africa; Swedish Research Council (VR) and Knut & Alice Wallenberg Foundation (KAW), Sweden; European Organization for Nuclear Research, Switzerland; Suranaree University of Technology (SUT), National Science and Technology Development Agency (NSTDA) and National Science, Research and Innovation Fund (NSRF via PMU-B B05F650021), Thailand; Turkish Energy, Nuclear and Mineral Research Agency (TENMAK), Turkey; National Academy of Sciences of Ukraine, Ukraine; Science and Technology Facilities Council (STFC), United Kingdom; National Science Foundation of the United States of America (NSF) and United States Department of

Energy, Office of Nuclear Physics (DOE NP), United States of America. In addition, individual groups or members have received support from: Czech Science Foundation (grant no. 23-07499S), Czech Republic; FORTE project, reg. no. CZ.02.01.01/00/22_008/0004632, Czech Republic, co-funded by the European Union, Czech Republic; European Research Council (grant no. 950692), European Union; Deutsche Forschungs Gemeinschaft (DFG, German Research Foundation) “Neutrinos and Dark Matter in Astro- and Particle Physics” (grant no. SFB 1258), Germany; ICSC - National Research Center for High Performance Computing, Big Data and Quantum Computing and FAIR - Future Artificial Intelligence Research, funded by the NextGenerationEU program (Italy).

References

- [1] B. A. Kniehl, G. Kramer, I. Schienbein, and H. Spiesberger, “Finite-mass effects on inclusive B meson hadroproduction”, *Phys. Rev. D* **77** (2008) 014011, arXiv:0705.4392 [hep-ph].
- [2] M. Cacciari, S. Frixione, M. L. Mangano, P. Nason, and G. Ridolfi, “QCD analysis of first b cross-section data at 1.96-TeV”, *JHEP* **07** (2004) 033, arXiv:hep-ph/0312132.
- [3] B. A. Kniehl, G. Kramer, I. Schienbein, and H. Spiesberger, “Collinear subtractions in hadroproduction of heavy quarks”, *Eur. Phys. J. C* **41** (2005) 199–212, arXiv:hep-ph/0502194.
- [4] M. Cacciari and P. Nason, “Charm cross-sections for the Tevatron Run II”, *JHEP* **09** (2003) 006, arXiv:hep-ph/0306212.
- [5] M. Cacciari, G. P. Salam, and G. Soyez, “The anti- k_t jet clustering algorithm”, *JHEP* **04** (2008) 063, arXiv:0802.1189 [hep-ph].
- [6] M. Cacciari, G. P. Salam, and G. Soyez, “FastJet User Manual”, *Eur. Phys. J. C* **72** (2012) 1896, arXiv:1111.6097 [hep-ph].
- [7] **ALICE** Collaboration, K. Aamodt *et al.*, “Particle-yield modification in jet-like azimuthal di-hadron correlations in Pb–Pb collisions at $\sqrt{s_{\text{NN}}} = 2.76$ TeV”, *Phys. Rev. Lett.* **108** (2012) 092301, arXiv:1110.0121 [nucl-ex].
- [8] **ALICE** Collaboration, J. Adam *et al.*, “Jet-like correlations with neutral pion triggers in pp and central Pb–Pb collisions at $\sqrt{s_{\text{NN}}} = 2.76$ TeV”, *Phys. Lett. B* **763** (2016) 238–250, arXiv:1608.07201 [nucl-ex].
- [9] **ALICE** Collaboration, J. Adam *et al.*, “Measurement of azimuthal correlations of D mesons and charged particles in pp collisions at $\sqrt{s} = 7$ TeV and p–Pb collisions at $\sqrt{s_{\text{NN}}} = 5.02$ TeV”, *Eur. Phys. J. C* **77** (2017) 245, arXiv:1605.06963 [nucl-ex].
- [10] **ALICE** Collaboration, S. Acharya *et al.*, “Azimuthal correlations of prompt D mesons with charged particles in pp and p–Pb collisions at $\sqrt{s_{\text{NN}}} = 5.02$ TeV”, *Eur. Phys. J. C* **80** (2020) 979, arXiv:1910.14403 [nucl-ex].
- [11] **ALICE** Collaboration, S. Acharya *et al.*, “Azimuthal correlations of heavy-flavor hadron decay electrons with charged particles in pp and p–Pb collisions at $\sqrt{s_{\text{NN}}} = 5.02$ TeV”, *Eur. Phys. J. C* **83** (2023) 741, arXiv:2303.00591 [nucl-ex].
- [12] M. L. Mangano, P. Nason, and G. Ridolfi, “Heavy quark correlations in hadron collisions at next-to-leading order”, *Nucl. Phys. B* **373** (1992) 295–345.
- [13] E. Norrbin and T. Sjostrand, “Production and hadronization of heavy quarks”, *Eur. Phys. J. C* **17** (2000) 137–161, arXiv:hep-ph/0005110.

- [14] F. Kheyri, M. Khodadi, and H. R. Sepangi, “Horava-Lifshitz early universe phase transition beyond detailed balance”, *Eur. Phys. J. C* **73** (2013) 2286, arXiv:1301.5460 [gr-qc].
- [15] A. Bazavov *et al.*, “The chiral and deconfinement aspects of the QCD transition”, *Phys. Rev. D* **85** (2012) 054503, arXiv:1111.1710 [hep-lat].
- [16] S. Borsanyi, G. Endrodi, Z. Fodor, A. Jakovac, S. D. Katz, S. Krieg, C. Ratti, and K. K. Szabo, “The QCD equation of state with dynamical quarks”, *JHEP* **11** (2010) 077, arXiv:1007.2580 [hep-lat].
- [17] **HotQCD** Collaboration, A. Bazavov *et al.*, “Chiral crossover in QCD at zero and non-zero chemical potentials”, *Phys. Lett. B* **795** (2019) 15–21, arXiv:1812.08235 [hep-lat].
- [18] A. Bazavov *et al.*, “Equation of state and QCD transition at finite temperature”, *Phys. Rev. D* **80** (2009) 014504, arXiv:0903.4379 [hep-lat].
- [19] B. Muller, J. Schukraft, and B. Wyslouch, “First Results from Pb+Pb collisions at the LHC”, *Ann. Rev. Nucl. Part. Sci.* **62** (2012) 361–386, arXiv:1202.3233 [hep-ex].
- [20] **ALICE** Collaboration, S. Acharya *et al.*, “The ALICE experiment: a journey through QCD”, *Eur. Phys. J. C* **84** (2024) 813, arXiv:2211.04384 [nucl-ex].
- [21] **BRAHMS** Collaboration, I. Arsene *et al.*, “Quark gluon plasma and color glass condensate at RHIC? The Perspective from the BRAHMS experiment”, *Nucl. Phys. A* **757** (2005) 1–27, arXiv:nucl-ex/0410020.
- [22] **PHOBOS** Collaboration, B. B. Back *et al.*, “The PHOBOS perspective on discoveries at RHIC”, *Nucl. Phys. A* **757** (2005) 28–101, arXiv:nucl-ex/0410022.
- [23] **STAR** Collaboration, J. Adams *et al.*, “Experimental and theoretical challenges in the search for the quark gluon plasma: The STAR Collaboration’s critical assessment of the evidence from RHIC collisions”, *Nucl. Phys. A* **757** (2005) 102–183, arXiv:nucl-ex/0501009.
- [24] **PHENIX** Collaboration, K. Adcox *et al.*, “Formation of dense partonic matter in relativistic nucleus-nucleus collisions at RHIC: Experimental evaluation by the PHENIX collaboration”, *Nucl. Phys. A* **757** (2005) 184–283, arXiv:nucl-ex/0410003.
- [25] R. Baier, D. Schiff, and B. G. Zakharov, “Energy loss in perturbative QCD”, *Ann. Rev. Nucl. Part. Sci.* **50** (2000) 37–69, arXiv:hep-ph/0002198.
- [26] Y. L. Dokshitzer and D. E. Kharzeev, “Heavy quark colorimetry of QCD matter”, *Phys. Lett. B* **519** (2001) 199–206, arXiv:hep-ph/0106202.
- [27] N. Armesto, C. A. Salgado, and U. A. Wiedemann, “Medium induced gluon radiation off massive quarks fills the dead cone”, *Phys. Rev. D* **69** (2004) 114003, arXiv:hep-ph/0312106.
- [28] S. Wicks, W. Horowitz, M. Djordjevic, and M. Gyulassy, “Heavy quark jet quenching with collisional plus radiative energy loss and path length fluctuations”, *Nucl. Phys. A* **783** (2007) 493–496, arXiv:nucl-th/0701063.
- [29] B.-W. Zhang, E. Wang, and X.-N. Wang, “Heavy quark energy loss in nuclear medium”, *Phys. Rev. Lett.* **93** (2004) 072301, arXiv:nucl-th/0309040.
- [30] A. Adil and I. Vitev, “Collisional dissociation of heavy mesons in dense QCD matter”, *Phys. Lett. B* **649** (2007) 139–146, arXiv:hep-ph/0611109.

- [31] G.-Y. Qin and X.-N. Wang, “Jet quenching in high-energy heavy-ion collisions”, *Int. J. Mod. Phys. E* **24** (2015) 1530014, arXiv:1511.00790 [hep-ph].
- [32] J.-P. Blaizot, Y. Mehtar-Tani, and M. A. C. Torres, “Angular structure of the in-medium QCD cascade”, *Phys. Rev. Lett.* **114** (2015) 222002, arXiv:1407.0326 [hep-ph].
- [33] ATLAS Collaboration, M. Aaboud *et al.*, “Measurement of jet fragmentation in Pb+Pb and $p\bar{p}$ collisions at $\sqrt{s_{NN}} = 5.02$ TeV with the ATLAS detector”, *Phys. Rev. C* **98** (2018) 024908, arXiv:1805.05424 [nucl-ex].
- [34] CMS Collaboration, S. Chatrchyan *et al.*, “Measurement of Jet Fragmentation in PbPb and $p\bar{p}$ Collisions at $\sqrt{s_{NN}} = 2.76$ TeV”, *Phys. Rev. C* **90** (2014) 024908, arXiv:1406.0932 [nucl-ex].
- [35] S. Cao and G.-Y. Qin, “Medium Response and Jet–Hadron Correlations in Relativistic Heavy-Ion Collisions”, *Ann. Rev. Nucl. Part. Sci.* **73** (2023) 205–229, arXiv:2211.16821 [nucl-th].
- [36] Y. Li, S.-Y. Chen, W.-X. Kong, S. Wang, and B.-W. Zhang, “Medium Modifications of Heavy-Flavor Jet Angularities in High-Energy Nuclear Collisions”, *Chin. Phys. Lett.* **42** (2025) 011201, arXiv:2409.12742 [hep-ph].
- [37] G. Y. Qin, A. Majumder, H. Song, and U. Heinz, “Energy and momentum deposited into a QCD medium by a jet shower”, *Phys. Rev. Lett.* **103** (2009) 152303, arXiv:0903.2255 [nucl-th].
- [38] J. Casalderrey-Solana, J. G. Milhano, D. Pablos, K. Rajagopal, and X. Yao, “Jet Wake from Linearized Hydrodynamics”, *JHEP* **05** (2021) 230, arXiv:2010.01140 [hep-ph].
- [39] Z. Yang and X.-N. Wang, “Rapidity asymmetry of jet-hadron correlation as a robust signal of diffusion wake induced by di-jets in high-energy heavy-ion collisions”, arXiv:2501.03419 [hep-ph].
- [40] Z. Yang, T. Luo, W. Chen, L.-G. Pang, and X.-N. Wang, “3D Structure of Jet-Induced Diffusion Wake in an Expanding Quark-Gluon Plasma”, *Phys. Rev. Lett.* **130** (2023) 052301, arXiv:2203.03683 [hep-ph].
- [41] W. Chen, Z. Yang, L. Pang, Y. He, T. Luo, and X. N. Wang, “The Signals of Jet-induced Diffusion Wake on Z/γ -hadron Correlations in High-Energy Heavy-Ion Collisions”, *Acta Phys. Polon. Supp.* **16** (2023) 1–A53.
- [42] M. Djordjevic, M. Gyulassy, and S. Wicks, “The Charm and beauty of RHIC and LHC”, *Phys. Rev. Lett.* **94** (2005) 112301, arXiv:hep-ph/0410372.
- [43] ALICE Collaboration, S. Acharya *et al.*, “Measurements of low- p_T electrons from semileptonic heavy-flavour hadron decays at mid-rapidity in $p\bar{p}$ and Pb–Pb collisions at $\sqrt{s_{NN}} = 2.76$ TeV”, *JHEP* **10** (2018) 061, arXiv:1805.04379 [nucl-ex].
- [44] ALICE Collaboration, S. Acharya *et al.*, “Measurement of D^0 , D^+ , D^{*+} and D_s^+ production in Pb–Pb collisions at $\sqrt{s_{NN}} = 5.02$ TeV”, *JHEP* **10** (2018) 174, arXiv:1804.09083 [nucl-ex].
- [45] ALICE Collaboration, B. Abelev *et al.*, “Suppression of high transverse momentum D mesons in central Pb–Pb collisions at $\sqrt{s_{NN}} = 2.76$ TeV”, *JHEP* **09** (2012) 112, arXiv:1203.2160 [nucl-ex].
- [46] CMS Collaboration, A. M. Sirunyan *et al.*, “Nuclear modification factor of D^0 mesons in PbPb collisions at $\sqrt{s_{NN}} = 5.02$ TeV”, *Phys. Lett. B* **782** (2018) 474–496, arXiv:1708.04962 [nucl-ex].

- [47] **ALICE** Collaboration, S. Acharya *et al.*, “Measurement of beauty production via non-prompt D^0 mesons in Pb–Pb collisions at $\sqrt{s_{\text{NN}}} = 5.02 \text{ TeV}$ ”, *JHEP* **12** (2022) 126, arXiv:2202.00815 [nucl-ex].
- [48] **ALICE** Collaboration, S. Acharya *et al.*, “Measurement of electrons from beauty-hadron decays in pp and Pb–Pb collisions at $\sqrt{s_{\text{NN}}} = 5.02 \text{ TeV}$ ”, *Phys. Rev. C* **108** (2023) 034906, arXiv:2211.13985 [nucl-ex].
- [49] **ATLAS** Collaboration, G. Aad *et al.*, “Measurement of the nuclear modification factor for muons from charm and bottom hadrons in Pb+Pb collisions at 5.02 TeV with the ATLAS detector”, *Phys. Lett. B* **829** (2022) 137077, arXiv:2109.00411 [nucl-ex].
- [50] **CMS** Collaboration, S. Chatrchyan *et al.*, “Evidence of b-Jet Quenching in PbPb Collisions at $\sqrt{s_{\text{NN}}} = 2.76 \text{ TeV}$ ”, *Phys. Rev. Lett.* **113** (2014) 132301, arXiv:1312.4198 [nucl-ex]. [Erratum: Phys.Rev.Lett. 115, 029903 (2015)].
- [51] **ATLAS** Collaboration, G. Aad *et al.*, “Measurement of the nuclear modification factor of b -jets in 5.02 TeV Pb+Pb collisions with the ATLAS detector”, *Eur. Phys. J. C* **83** (2023) 438, arXiv:2204.13530 [nucl-ex].
- [52] **CMS** Collaboration, A. Tumasyan *et al.*, “Search for medium effects using jets from bottom quarks in PbPb collisions at $\sqrt{s_{\text{NN}}} = 5.02 \text{ TeV}$ ”, *Phys. Lett. B* **844** (2023) 137849, arXiv:2210.08547 [hep-ex].
- [53] **ALICE** Collaboration, S. Acharya *et al.*, “Jet-like correlations with respect to K_S^0 and Λ ($\bar{\Lambda}$) in pp and Pb–Pb collisions at $\sqrt{s_{\text{NN}}} = 5.02 \text{ TeV}$ ”, *Eur. Phys. J. C* **83** (2023) 497, arXiv:2211.01197 [nucl-ex].
- [54] **ALICE** Collaboration, S. Acharya *et al.*, “Measurements of jet quenching using semi-inclusive hadron+jet distributions in pp and central Pb–Pb collisions at $\sqrt{s_{\text{NN}}} = 5.02 \text{ TeV}$ ”, *Phys. Rev. C* **110** (2024) 014906, arXiv:2308.16128 [nucl-ex].
- [55] **ALICE** Collaboration, S. Acharya *et al.*, “Observation of Medium-Induced Yield Enhancement and Acoplanarity Broadening of Low- p_T Jets from Measurements in pp and Central Pb-Pb Collisions at $\sqrt{s_{\text{NN}}} = 5.02 \text{ TeV}$ ”, *Phys. Rev. Lett.* **133** (2024) 022301, arXiv:2308.16131 [nucl-ex].
- [56] J. Casalderrey-Solana, D. C. Gulhan, J. G. Milhano, D. Pablos, and K. Rajagopal, “A Hybrid Strong/Weak Coupling Approach to Jet Quenching”, *JHEP* **10** (2014) 019, arXiv:1405.3864 [hep-ph]. [Erratum: JHEP 09, 175 (2015)].
- [57] **PHENIX** Collaboration, A. Adare *et al.*, “Azimuthal correlations of electrons from heavy-flavor decay with hadrons in p+p and Au+Au collisions at $\sqrt{s_{\text{NN}}} = 200 \text{ GeV}$ ”, *Phys. Rev. C* **83** (2011) 044912, arXiv:1011.1477 [nucl-ex].
- [58] **STAR** Collaboration, J. Adam *et al.*, “Measurement of D^0 -meson + hadron two-dimensional angular correlations in Au+Au collisions at $\sqrt{s_{\text{NN}}} = 200 \text{ GeV}$ ”, *Phys. Rev. C* **102** (2020) 014905, arXiv:1911.12168 [nucl-ex].
- [59] **ALICE** Collaboration, B. B. Abelev *et al.*, “Performance of the ALICE Experiment at the CERN LHC”, *Int. J. Mod. Phys. A* **29** (2014) 1430044, arXiv:1402.4476 [nucl-ex].
- [60] **ALICE** Collaboration, K. Aamodt *et al.*, “The ALICE experiment at the CERN LHC”, *JINST* **3** (2008) S08002.

- [61] **ALICE** Collaboration, K. Aamodt *et al.*, “Alignment of the ALICE Inner Tracking System with cosmic-ray tracks”, *JINST* **5** (2010) P03003, arXiv:1001.0502 [physics.ins-det].
- [62] J. Alme *et al.*, “The ALICE TPC, a large 3-dimensional tracking device with fast readout for ultra-high multiplicity events”, *Nucl. Instrum. Meth. A* **622** (2010) 316–367, arXiv:1001.1950 [physics.ins-det].
- [63] H. Bethe, “Theory of the Passage of Fast Corpuscular Rays Through Matter”, *Annalen Phys.* **5** (1930) 325–400.
- [64] **ALEPH** Collaboration, D. Buskulic *et al.*, “Performance of the ALEPH detector at LEP”, *Nucl. Instrum. Meth. A* **360** (1995) 481–506.
- [65] **ALEPH** Collaboration, R. Assmann *et al.*, “Calibration of the ALEPH dE/dx”, ALEPH 94-116, PHYSIC 94-089. CERN Document Server.
- [66] **ALICE** Collaboration, P. Cortese *et al.*, “ALICE Electromagnetic Calorimeter Technical Design Report”, CERN-LHCC-2008-014.
- [67] **ALICE** Collaboration, J. Allen *et al.*, “ALICE DCal: An Addendum to the EMCal Technical Design Report Di-Jet and Hadron-Jet correlation measurements in ALICE”, CERN-LHCC-2010-011, ALICE-TDR-14-add-1.
- [68] **ALICE** Collaboration, E. Abbas *et al.*, “Performance of the ALICE VZERO system”, *JINST* **8** (2013) P10016, arXiv:1306.3130 [nucl-ex].
- [69] **ALICE** Collaboration, P. Cortese, “Performance of the ALICE Zero Degree Calorimeters and upgrade strategy”, *J. Phys. Conf. Ser.* **1162** (2019) 012006.
- [70] **ALICE** Collaboration, S. Acharya *et al.*, “Centrality determination in heavy ion collisions”, ALICE-PUBLIC-2018-011.
- [71] **Particle Data Group** Collaboration, S. Navas *et al.*, “Review of particle physics”, *Phys. Rev. D* **110** (2024) 030001.
- [72] **ALICE** Collaboration, S. Acharya *et al.*, “The ALICE definition of primary particles”, ALICE-PUBLIC-2017-005.
- [73] **ALICE** Collaboration, S. Acharya *et al.*, “Measurement of electrons from semileptonic heavy-flavour hadron decays at midrapidity in pp and Pb–Pb collisions at $\sqrt{s_{\text{NN}}} = 5.02 \text{ TeV}$ ”, *Phys. Lett. B* **804** (2020) 135377, arXiv:1910.09110 [nucl-ex].
- [74] **ALICE** Collaboration, S. Acharya *et al.*, “Performance of the ALICE Electromagnetic Calorimeter”, *JINST* **18** (2023) P08007, arXiv:2209.04216 [physics.ins-det].
- [75] T. Awes, F. Obenshain, F. Plasil, S. Saini, S. Sorensen, and G. Young, “A simple method of shower localization and identification in laterally segmented calorimeters”, *Nuclear Instruments and Methods in Physics Research Section A: Accelerators, Spectrometers, Detectors and Associated Equipment* **311** (1992) 130–138.
- [76] **ALICE** Collaboration, B. B. Abelev *et al.*, “Long-range angular correlations of π , K and p in p–Pb collisions at $\sqrt{s_{\text{NN}}} = 5.02 \text{ TeV}$ ”, *Phys. Lett. B* **726** (2013) 164–177, arXiv:1307.3237 [nucl-ex].
- [77] **ALICE** Collaboration, S. Acharya *et al.*, “Measurement of electrons from heavy-flavour hadron decays as a function of multiplicity in p–Pb collisions at $\sqrt{s_{\text{NN}}} = 5.02 \text{ TeV}$ ”, *JHEP* **02** (2020) 077, arXiv:1910.14399 [nucl-ex].

- [78] **ALICE** Collaboration, J. Adam *et al.*, “Measurement of the production of high- p_{T} electrons from heavy-flavour hadron decays in Pb–Pb collisions at $\sqrt{s_{\text{NN}}} = 2.76 \text{ TeV}$ ”, *Phys. Lett. B* **771** (2017) 467–481, arXiv:1609.07104 [nucl-ex].
- [79] **ALICE** Collaboration, J. Adam *et al.*, “Measurement of electrons from heavy-flavour hadron decays in p–Pb collisions at $\sqrt{s_{\text{NN}}} = 5.02 \text{ TeV}$ ”, *Phys. Lett. B* **754** (2016) 81–93, arXiv:1509.07491 [nucl-ex].
- [80] X.-N. Wang and M. Gyulassy, “HIJING: A Monte Carlo model for multiple jet production in pp, pA and AA collisions”, *Phys. Rev. D* **44** (1991) 3501–3516.
- [81] R. Brun, F. Bruyant, F. Carminati, S. Giani, M. Maire, A. McPherson, G. Patrick, and L. Urban, “GEANT Detector Description and Simulation Tool”, CERN-W5013, CERN-W-5013, W5013, W-5013.
- [82] T. Sjostrand, S. Mrenna, and P. Z. Skands, “PYTHIA 6.4 Physics and Manual”, *JHEP* **05** (2006) 026, arXiv:hep-ph/0603175.
- [83] **ALICE** Collaboration, B. Abelev *et al.*, “Measurement of electrons from semileptonic heavy-flavour hadron decays in pp collisions at $\sqrt{s} = 7 \text{ TeV}$ ”, *Phys. Rev. D* **86** (2012) 112007, arXiv:1205.5423 [hep-ex].
- [84] **ALICE** Collaboration, K. Aamodt *et al.*, “Harmonic decomposition of two-particle angular correlations in Pb–Pb collisions at $\sqrt{s_{\text{NN}}} = 2.76 \text{ TeV}$ ”, *Phys. Lett. B* **708** (2012) 249–264, arXiv:1109.2501 [nucl-ex].
- [85] **ATLAS** Collaboration, G. Aad *et al.*, “Measurement of azimuthal anisotropy of muons from charm and bottom hadrons in Pb+Pb collisions at $\sqrt{s_{\text{NN}}} = 5.02 \text{ TeV}$ with the ATLAS detector”, *Phys. Lett. B* **807** (2020) 135595, arXiv:2003.03565 [nucl-ex].
- [86] **ALICE** Collaboration, S. Acharya *et al.*, “Energy dependence and fluctuations of anisotropic flow in Pb–Pb collisions at $\sqrt{s_{\text{NN}}} = 5.02$ and 2.76 TeV ”, *JHEP* **07** (2018) 103, arXiv:1804.02944 [nucl-ex].
- [87] **ALICE** Collaboration, S. Acharya *et al.*, “Transverse momentum spectra and nuclear modification factors of charged particles in pp, p–Pb and Pb–Pb collisions at the LHC”, *JHEP* **11** (2018) 013, arXiv:1802.09145 [nucl-ex].
- [88] R. A. Fisher, “Dispersion on a sphere”, *Proceedings of the Royal Society of London. Series A. Mathematical and Physical Sciences* **217** (1953) 295–305.
- [89] I. Vitev, “Large angle hadron correlations from medium-induced gluon radiation”, *Phys. Lett. B* **630** (2005) 78–84, arXiv:hep-ph/0501255.
- [90] **PHENIX** Collaboration, A. Adare *et al.*, “Dihadron azimuthal correlations in Au+Au collisions at $\sqrt{s_{\text{NN}}} = 200 \text{ GeV}$ ”, *Phys. Rev. C* **78** (2008) 014901, arXiv:0801.4545 [nucl-ex].
- [91] I. Vitev and M. Gyulassy, “High p_{T} tomography of $d + \text{Au}$ and Au+Au at SPS, RHIC, and LHC”, *Phys. Rev. Lett.* **89** (2002) 252301, arXiv:hep-ph/0209161.
- [92] B. Z. Kopeliovich, J. Nemchik, A. Schafer, and A. V. Tarasov, “Cronin effect in hadron production off nuclei”, *Phys. Rev. Lett.* **88** (2002) 232303, arXiv:hep-ph/0201010.
- [93] X.-N. Wang, “Systematic study of high p_{T} hadron spectra in pp, p A and A A collisions from SPS to RHIC energies”, *Phys. Rev. C* **61** (2000) 064910, arXiv:nucl-th/9812021.

- [94] G.-L. Ma and X.-N. Wang, “Jets, Mach cone, hot spots, ridges, harmonic flow, dihadron and γ -hadron correlation in high-energy heavy-ion collisions”, *Phys. Rev. Lett.* **106** (2011) 162301, arXiv:1011.5249 [nucl-th].
- [95] ALICE Collaboration, B. B. Abelev *et al.*, “Beauty production in pp collisions at $\sqrt{s} = 2.76$ TeV measured via semi-electronic decays”, *Phys. Lett. B* **738** (2014) 97–108, arXiv:1405.4144 [nucl-ex].
- [96] M. Cacciari, S. Frixione, N. Houdeau, M. L. Mangano, P. Nason, and G. Ridolfi, “Theoretical predictions for charm and bottom production at the LHC”, *JHEP* **10** (2012) 137, arXiv:1205.6344 [hep-ph].
- [97] ALICE Collaboration, S. Acharya *et al.*, “Prompt D^0 , D^+ , and D^{*+} production in Pb–Pb collisions at $\sqrt{s_{\text{NN}}} = 5.02$ TeV”, *JHEP* **01** (2022) 174, arXiv:2110.09420 [nucl-ex].
- [98] ALICE Collaboration, S. Acharya *et al.*, “ALICE upgrades during the LHC Long Shutdown 2”, *JINST* **19** (2024) P05062, arXiv:2302.01238 [physics.ins-det].

A Supplemental Figures

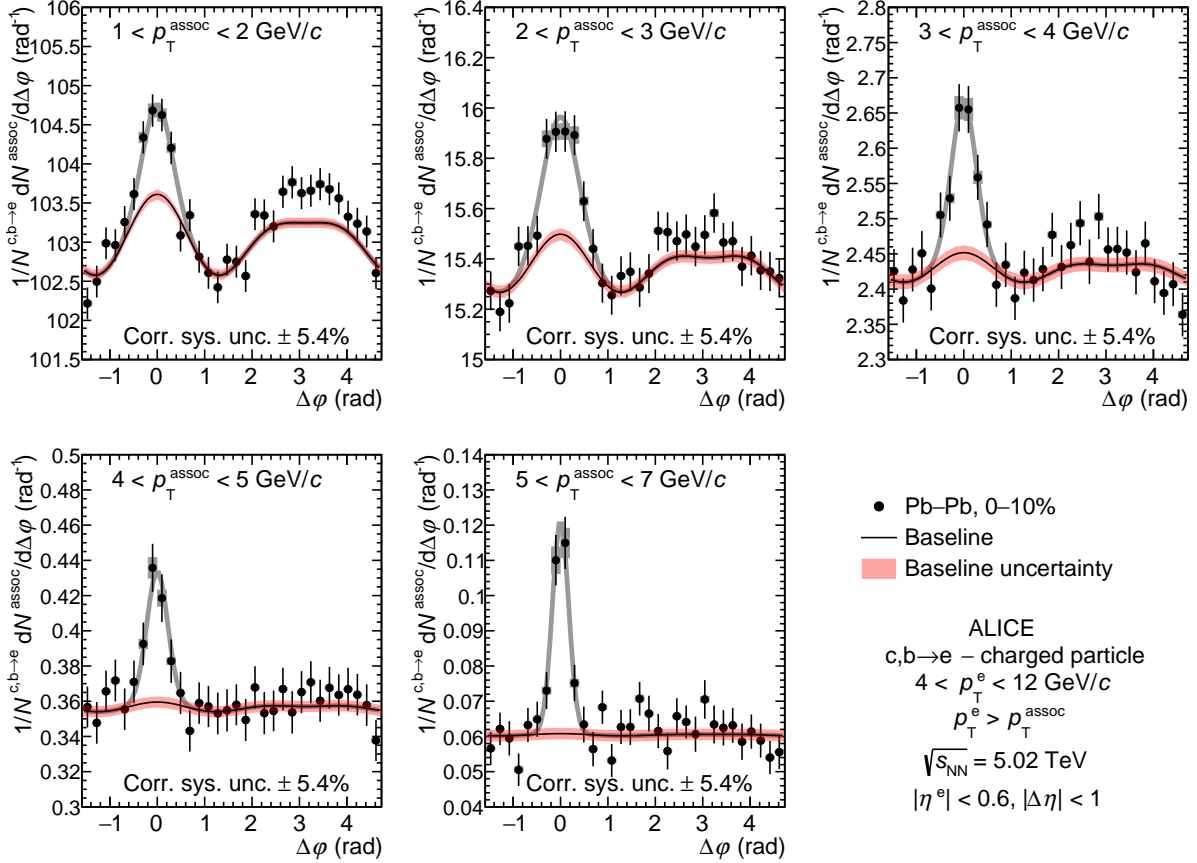


Figure A.1: Azimuthal-correlation distribution of electrons from heavy-flavor hadron decays and charged particles measured in 0–10% central Pb–Pb collisions before background subtraction. The distributions are shown in the trigger range of $4 < p_T^e < 12 \text{ GeV}/c$ and all p_T^{assoc} intervals, where $1–2$, $2–3$, and $5–7 \text{ GeV}/c$ are shown in Fig. 1.

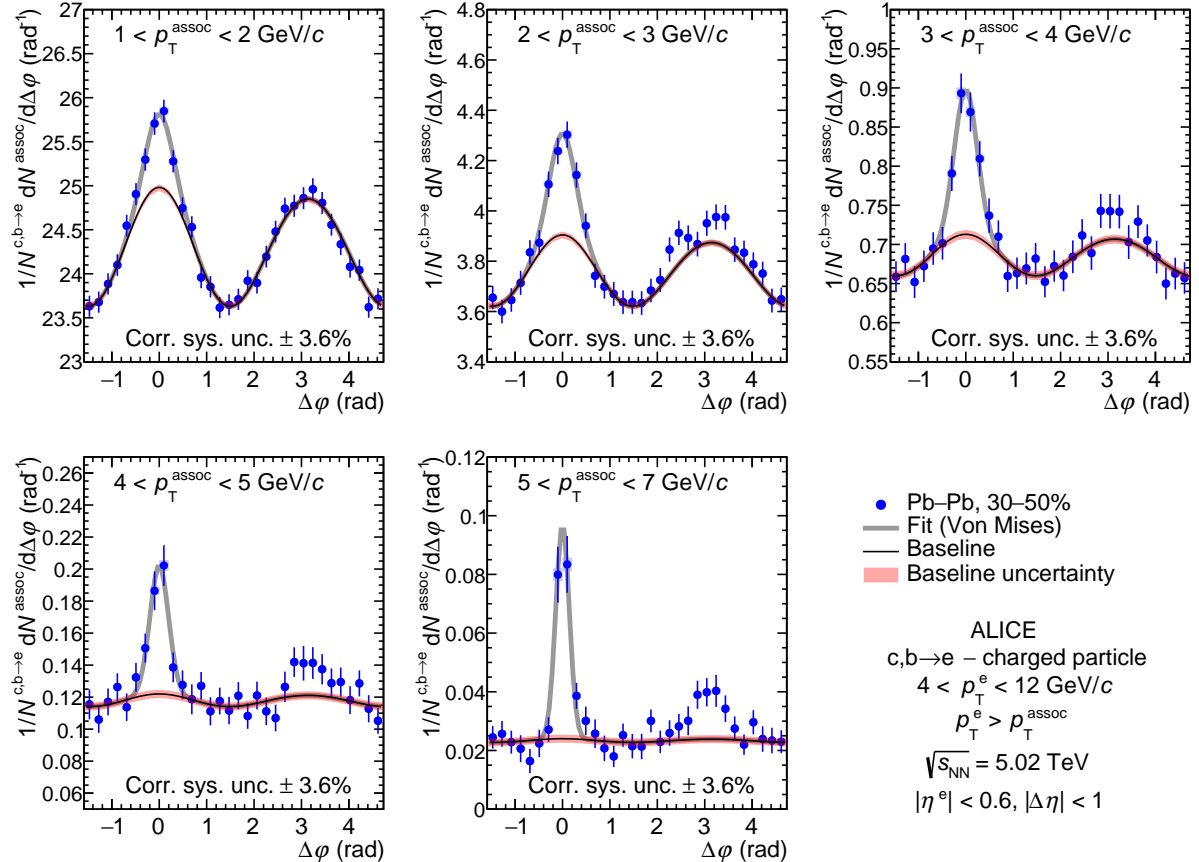


Figure A.2: Azimuthal-correlation distribution of electrons from heavy-flavor hadron decays and charged particles measured in 30–50% central Pb–Pb collisions before background subtraction. The distributions are shown in the trigger range of $4 < p_T^e < 12 \text{ GeV}/c$ and all p_T^{assoc} intervals, where $1 - 2$, $2 - 3$, and $5 - 7 \text{ GeV}/c$ are shown in Fig. 1.

B The ALICE Collaboration

- I.J. Abualrob ¹¹⁴, S. Acharya ⁵⁰, G. Aglieri Rinella ³², L. Aglietta ²⁴, M. Agnello ²⁹, N. Agrawal ²⁵, Z. Ahammed ¹³³, S. Ahmad ¹⁵, I. Ahuja ³⁶, ZUL. Akbar⁸¹, A. Akindinov ¹³⁹, V. Akishina³⁸, M. Al-Turany ⁹⁶, D. Aleksandrov ¹³⁹, B. Alessandro ⁵⁶, H.M. Alfanda ⁶, R. Alfaro Molina ⁶⁷, B. Ali ¹⁵, A. Alici ²⁵, A. Alkin ¹⁰³, J. Alme ²⁰, G. Alocco ²⁴, T. Alt ⁶⁴, A.R. Altamura ⁵⁰, I. Altsybeev ⁹⁴, C. Andrei ⁴⁵, N. Andreou ¹¹³, A. Andronic ¹²⁴, E. Andronov ¹³⁹, V. Anguelov ⁹³, F. Antinori ⁵⁴, P. Antonioli ⁵¹, N. Apadula ⁷³, H. Appelshäuser ⁶⁴, C. Arata ⁷², S. Arcelli ²⁵, R. Arnaldi ⁵⁶, J.G.M.C.A. Arneiro ¹⁰⁹, I.C. Arsene ¹⁹, M. Arslandok ¹³⁶, A. Augustinus ³², R. Averbeck ⁹⁶, M.D. Azmi ¹⁵, H. Baba¹²², A.R.J. Babu¹³⁵, A. Badalà ⁵³, J. Bae ¹⁰³, Y. Bae ¹⁰³, Y.W. Baek ⁴⁰, X. Bai ¹¹⁸, R. Bailhache ⁶⁴, Y. Bailung ⁴⁸, R. Bala ⁹⁰, A. Baldissari ¹²⁸, B. Balis ², S. Bangalia¹¹⁶, Z. Banoo ⁹⁰, V. Barbasova ³⁶, F. Barile ³¹, L. Barioglio ⁵⁶, M. Barlou ^{24,77}, B. Barman ⁴¹, G.G. Barnaföldi ⁴⁶, L.S. Barnby ¹¹³, E. Barreau ¹⁰², V. Barret ¹²⁵, L. Barreto ¹⁰⁹, K. Barth ³², E. Bartsch ⁶⁴, N. Bastid ¹²⁵, G. Batigne ¹⁰², D. Battistini ⁹⁴, B. Batyunya ¹⁴⁰, D. Bauri⁴⁷, J.L. Bazo Alba ¹⁰⁰, I.G. Bearden ⁸², P. Becht ⁹⁶, D. Behera ⁴⁸, S. Behera ⁴⁷, I. Belikov ¹²⁷, V.D. Bella ¹²⁷, F. Bellini ²⁵, R. Bellwied ¹¹⁴, L.G.E. Beltran ¹⁰⁸, Y.A.V. Beltran ⁴⁴, G. Bencedi ⁴⁶, A. Bensaoula ¹¹⁴, S. Beole ²⁴, Y. Berdnikov ¹³⁹, A. Berdnikova ⁹³, L. Bergmann ⁹³, L. Bernardinis ²³, L. Betev ³², P.P. Bhaduri ¹³³, T. Bhalla⁸⁹, A. Bhasin ⁹⁰, B. Bhattacharjee ⁴¹, S. Bhattacharai¹¹⁶, L. Bianchi ²⁴, J. Bielčík ³⁴, J. Bielčíková ⁸⁵, A. Bilandzic ⁹⁴, A. Binoy ¹¹⁶, G. Biro ⁴⁶, S. Biswas ⁴, D. Blau ¹³⁹, M.B. Blidaru ⁹⁶, N. Bluhme³⁸, C. Blume ⁶⁴, F. Bock ⁸⁶, T. Bodova ²⁰, J. Bok ¹⁶, L. Boldizsár ⁴⁶, M. Bombara ³⁶, P.M. Bond ³², G. Bonomi ^{132,55}, H. Borel ¹²⁸, A. Borissov ¹³⁹, A.G. Borquez Carcamo ⁹³, E. Botta ²⁴, Y.E.M. Bouziani ⁶⁴, D.C. Brandibur ⁶³, L. Bratrud ⁶⁴, P. Braun-Munzinger ⁹⁶, M. Bregant ¹⁰⁹, M. Broz ³⁴, G.E. Bruno ^{95,31}, V.D. Buchakchiev ³⁵, M.D. Buckland ⁸⁴, H. Buesching ⁶⁴, S. Bufalino ²⁹, P. Buhler ¹⁰¹, N. Burmasov ¹⁴⁰, Z. Buthelezi ^{68,121}, A. Bylinkin ²⁰, C. Carr ⁹⁹, J.C. Cabanillas Noris ¹⁰⁸, M.F.T. Cabrera ¹¹⁴, H. Caines ¹³⁶, A. Caliva ²⁸, E. Calvo Villar ¹⁰⁰, J.M.M. Camacho ¹⁰⁸, P. Camerini ²³, M.T. Camerlingo ⁵⁰, F.D.M. Canedo ¹⁰⁹, S. Cannito ²³, S.L. Cantway ¹³⁶, M. Carabas ¹¹², F. Carnesecchi ³², L.A.D. Carvalho ¹⁰⁹, J. Castillo Castellanos ¹²⁸, M. Castoldi ³², F. Catalano ³², S. Cattaruzzi ²³, R. Cerri ²⁴, I. Chakaberia ⁷³, P. Chakraborty ¹³⁴, J.W.O. Chan^{1,114}, S. Chandra ¹³³, S. Chapeland ³², M. Chartier ¹¹⁷, S. Chattopadhyay ¹³³, M. Chen ³⁹, T. Cheng ⁶, C. Cheshkov ¹²⁶, D. Chiappara ²⁷, V. Chibante Barroso ³², D.D. Chinellato ¹⁰¹, F. Chinu ²⁴, E.S. Chizzali ^{II,94}, J. Cho ⁵⁸, S. Cho ⁵⁸, P. Chochula ³², Z.A. Chochulska ^{III,134}, D. Choudhury⁴¹, P. Christakoglou ⁸³, C.H. Christensen ⁸², P. Christiansen ⁷⁴, T. Chujo ¹²³, M. Ciacco ²⁹, C. Cicalo ⁵², G. Cimador ²⁴, F. Cindolo ⁵¹, M.R. Ciupek⁹⁶, G. Clai^{IV,51}, F. Colamaria ⁵⁰, J.S. Colburn⁹⁹, D. Colella ³¹, A. Colelli³¹, M. Colocci ²⁵, M. Concas ³², G. Conesa Balbastre ⁷², Z. Conesa del Valle ¹²⁹, G. Contin ²³, J.G. Contreras ³⁴, M.L. Coquet ¹⁰², P. Cortese ^{131,56}, M.R. Cosentino ¹¹¹, F. Costa ³², S. Costanza ²¹, P. Crochet ¹²⁵, M.M. Czarnynoga¹³⁴, A. Dainese ⁵⁴, G. Dange³⁸, M.C. Danisch ⁹³, A. Danu ⁶³, P. Das ³², S. Das ⁴, A.R. Dash ¹²⁴, S. Dash ⁴⁷, A. De Caro ²⁸, G. de Cataldo ⁵⁰, J. de Cuveland ³⁸, A. De Falco ²², D. De Gruttola ²⁸, N. De Marco ⁵⁶, C. De Martin ²³, S. De Pasquale ²⁸, R. Deb ¹³², R. Del Grande ⁹⁴, L. Dello Stritto ³², G.G.A. de Souza ^{V,109}, P. Dhankher ¹⁸, D. Di Bari ³¹, M. Di Costanzo ²⁹, A. Di Mauro ³², B. Di Ruzza ¹³⁰, B. Diab ³², Y. Ding ⁶, J. Ditzel ⁶⁴, R. Divià ³², Ø. Djupsland²⁰, A. Dobrin ⁶³, B. Dönigus ⁶⁴, L. Döpper ⁴², J.M. Dubinski ¹³⁴, A. Dubla ⁹⁶, P. Dupieux ¹²⁵, N. Dzalaiova¹³, T.M. Eder ¹²⁴, R.J. Ehlers ⁷³, F. Eisenhut ⁶⁴, R. Ejima ⁹¹, D. Elia ⁵⁰, B. Erazmus ¹⁰², F. Ercolelli ²⁵, B. Espagnon ¹²⁹, G. Eulisse ³², D. Evans ⁹⁹, L. Fabbietti ⁹⁴, M. Faggion ³², J. Faivre ⁷², F. Fan ⁶, W. Fan ⁷³, T. Fang⁶, A. Fantoni ⁴⁹, M. Fasel ⁸⁶, G. Feofilov ¹³⁹, A. Fernández Téllez ⁴⁴, L. Ferrandi ¹⁰⁹, M.B. Ferrer ³², A. Ferrero ¹²⁸, C. Ferrero ^{VI,56}, A. Ferretti ²⁴, V.J.G. Feuillard ⁹³, D. Finogeev ¹⁴⁰, F.M. Fionda ⁵², A.N. Flores ¹⁰⁷, S. Foertsch ⁶⁸, I. Fokin ⁹³, S. Fokin ¹³⁹, U. Follo ^{VI,56}, R. Forynski ¹¹³, E. Fragiocomo ⁵⁷, E. Frajna ⁴⁶, H. Friberg ⁹⁴, U. Fuchs ³², N. Funicello ²⁸, C. Furget ⁷², A. Furs ¹⁴⁰, T. Fusayasu ⁹⁷, J.J. Gaardhøje ⁸², M. Gagliardi ²⁴, A.M. Gago ¹⁰⁰, T. Gahlaud⁴⁷, C.D. Galvan ¹⁰⁸, S. Gami ⁷⁹, D.R. Gangadharan ¹¹⁴, P. Ganoti ⁷⁷, C. Garabatos ⁹⁶, J.M. Garcia ⁴⁴, T. García Chávez ⁴⁴, E. Garcia-Solis ⁹, S. Garetti ¹²⁹, C. Gargiulo ³², P. Gasik ⁹⁶, H.M. Gaur³⁸, A. Gautam ¹¹⁶, M.B. Gay Ducati ⁶⁶, M. Germain ¹⁰², R.A. Gernhaeuser ⁹⁴, C. Ghosh¹³³, M. Giacalone ⁵¹, G. Gioachin ²⁹, S.K. Giri ¹³³, P. Giubellino ^{96,56}, P. Giubilato ²⁷, P. Glässel ⁹³, E. Glimos ¹²⁰, V. Gonzalez ¹³⁵, M. Gorgon ², K. Goswami ⁴⁸, S. Gotovac ³³, V. Grabski ⁶⁷, L.K. Graczykowski ¹³⁴, E. Grecka ⁸⁵, A. Grelli ⁵⁹, C. Grigoras ³², V. Grigoriev ¹³⁹, S. Grigoryan ^{140,1}, O.S. Groettvik ³², F. Grossa ³², J.F. Grosse-Oetringhaus ³², R. Grossi ⁹⁶, D. Grund ³⁴, N.A. Grunwald ⁹³, R. Guernane ⁷², M. Guilbaud ¹⁰², K. Gulbrandsen ⁸²,

- J.K. Gumprecht ¹⁰¹, T. Gündem ⁶⁴, T. Gunji ¹²², J. Guo¹⁰, W. Guo ⁶, A. Gupta ⁹⁰, R. Gupta ⁹⁰, R. Gupta ⁴⁸, K. Gwizdziel ¹³⁴, L. Gyulai ⁴⁶, C. Hadjidakis ¹²⁹, F.U. Haider ⁹⁰, S. Haidlova ³⁴, M. Haldar⁴, H. Hamagaki ⁷⁵, Y. Han ¹³⁸, B.G. Hanley ¹³⁵, R. Hannigan ¹⁰⁷, J. Hansen ⁷⁴, J.W. Harris ¹³⁶, A. Harton ⁹, M.V. Hartung ⁶⁴, H. Hassan ¹¹⁵, D. Hatzifotiadou ⁵¹, P. Hauer ⁴², L.B. Havener ¹³⁶, E. Hellbär ³², H. Helstrup ³⁷, M. Hemmer ⁶⁴, T. Herman ³⁴, S.G. Hernandez¹¹⁴, G. Herrera Corral ⁸, K.F. Hetland ³⁷, B. Heybeck ⁶⁴, H. Hillemanns ³², B. Hippolyte ¹²⁷, I.P.M. Hobus ⁸³, F.W. Hoffmann ⁷⁰, B. Hofman ⁵⁹, M. Horst ⁹⁴, A. Horzyk ², Y. Hou ^{96,6}, P. Hristov ³², P. Huhn⁶⁴, L.M. Huhta ¹¹⁵, T.J. Humanic ⁸⁷, V. Humlova ³⁴, A. Hutson ¹¹⁴, D. Hutter ³⁸, M.C. Hwang ¹⁸, R. Ilkaev¹³⁹, M. Inaba ¹²³, M. Ippolitov ¹³⁹, A. Isakov ⁸³, T. Isidori ¹¹⁶, M.S. Islam ⁴⁷, M. Ivanov¹³, M. Ivanov ⁹⁶, K.E. Iversen ⁷⁴, J.G. Kim ¹³⁸, M. Jablonski ², B. Jacak ^{18,73}, N. Jacazio ²⁵, P.M. Jacobs ⁷³, S. Jadlovska¹⁰⁵, J. Jadlovsky ¹⁰⁵, S. Jaelani ⁸¹, C. Jahnke ¹¹⁰, M.J. Jakubowska ¹³⁴, D.M. Janik ³⁴, M.A. Janik ¹³⁴, S. Ji ¹⁶, S. Jia ⁸², T. Jiang ¹⁰, A.A.P. Jimenez ⁶⁵, S. Jin^{1,10}, F. Jonas ⁷³, D.M. Jones ¹¹⁷, J.M. Jowett ^{32,96}, J. Jung ⁶⁴, M. Jung ⁶⁴, A. Junique ³², A. Jusko ⁹⁹, J. Kaewjai¹⁰⁴, P. Kalinak ⁶⁰, A. Kalweit ³², A. Karasu Uysal ¹³⁷, N. Karatzenis⁹⁹, O. Karavichev ¹³⁹, T. Karavicheva ¹³⁹, M.J. Karwowska ¹³⁴, U. Kebschull ⁷⁰, M. Keil ³², B. Ketzer ⁴², J. Keul ⁶⁴, S.S. Khade ⁴⁸, A.M. Khan ¹¹⁸, A. Khanzadeev ¹³⁹, Y. Kharlov ¹³⁹, A. Khatun ¹¹⁶, A. Khuntia ⁵¹, Z. Khuranova ⁶⁴, B. Kileng ³⁷, B. Kim ¹⁰³, C. Kim ¹⁶, D.J. Kim ¹¹⁵, D. Kim ¹⁰³, E.J. Kim ⁶⁹, G. Kim ⁵⁸, H. Kim ⁵⁸, J. Kim ¹³⁸, J. Kim ⁵⁸, J. Kim ³², M. Kim ¹⁸, S. Kim ¹⁷, T. Kim ¹³⁸, K. Kimura ⁹¹, S. Kirsch ⁶⁴, I. Kisel ³⁸, S. Kiselev ¹³⁹, A. Kisiel ¹³⁴, J.L. Klay ⁵, J. Klein ³², S. Klein ⁷³, C. Klein-Bösing ¹²⁴, M. Kleiner ⁶⁴, A. Kluge ³², C. Kobdaj ¹⁰⁴, R. Kohara ¹²², T. Kollegger⁹⁶, A. Kondratyev ¹⁴⁰, N. Kondratyeva ¹³⁹, J. Konig ⁶⁴, P.J. Konopka ³², G. Kornakov ¹³⁴, M. Korwieser ⁹⁴, S.D. Koryciak ², C. Koster ⁸³, A. Kotliarov ⁸⁵, N. Kovacic ⁸⁸, V. Kovalenko ¹³⁹, M. Kowalski ¹⁰⁶, V. Kozhuharov ³⁵, G. Kozlov ³⁸, I. Králik ⁶⁰, A. Kravčáková ³⁶, L. Krcal ³², M. Krivda ^{99,60}, F. Krizek ⁸⁵, K. Krizkova Gajdosova ³⁴, C. Krug ⁶⁶, E. Kryshen ¹³⁹, V. Kučera ⁵⁸, C. Kuhn ¹²⁷, T. Kumaoka¹²³, D. Kumar ¹³³, L. Kumar ⁸⁹, N. Kumar⁸⁹, S. Kumar ⁵⁰, S. Kundu ³², M. Kuo¹²³, P. Kurashvili ⁷⁸, A.B. Kurepin ¹³⁹, S. Kurita ⁹¹, A. Kuryakin ¹³⁹, S. Kushpil ⁸⁵, M. Kutyla¹³⁴, A. Kuznetsov ¹⁴⁰, M.J. Kweon ⁵⁸, Y. Kwon ¹³⁸, S.L. La Pointe ³⁸, P. La Rocca ²⁶, A. Lakrathok ¹⁰⁴, M. Lamanna ³², S. Lambert¹⁰², A.R. Landou ⁷², R. Langoy ¹¹⁹, P. Larionov ³², E. Laudi ³², L. Lautner ⁹⁴, R.A.N. Laveaga ¹⁰⁸, R. Lavicka ¹⁰¹, R. Lea ^{132,55}, H. Lee ¹⁰³, I. Legrand ⁴⁵, G. Legras ¹²⁴, A.M. Lejeune ³⁴, T.M. Lelek ², R.C. Lemmon ^{1,84}, I. León Monzón ¹⁰⁸, M.M. Lesch ⁹⁴, P. Lévai ⁴⁶, M. Li⁶, P. Li¹⁰, X. Li¹⁰, B.E. Liang-Gilman ¹⁸, J. Lien ¹¹⁹, R. Lietava ⁹⁹, I. Likmeta ¹¹⁴, B. Lim ⁵⁶, H. Lim ¹⁶, S.H. Lim ¹⁶, S. Lin¹⁰, V. Lindenstruth ³⁸, C. Lippmann ⁹⁶, D. Liskova ¹⁰⁵, D.H. Liu ⁶, J. Liu ¹¹⁷, G.S.S. Liveraro ¹¹⁰, I.M. Lofnes ²⁰, C. Loizides ⁸⁶, S. Lokos ¹⁰⁶, J. Lömker ⁵⁹, X. Lopez ¹²⁵, E. López Torres ⁷, C. Lotteau ¹²⁶, P. Lu ^{96,118}, W. Lu ⁶, Z. Lu ¹⁰, F.V. Lugo ⁶⁷, J. Luo³⁹, G. Luparello ⁵⁷, M.A.T. Johnson ⁴⁴, Y.G. Ma ³⁹, M. Mager ³², A. Maire ¹²⁷, E.M. Majerz ², M.V. Makarieva ³⁵, G. Malfattore ⁵¹, N.M. Malik ⁹⁰, N. Malik ¹⁵, S.K. Malik ⁹⁰, D. Mallick ¹²⁹, N. Mallick ¹¹⁵, G. Mandaglio ^{30,53}, S.K. Mandal ⁷⁸, A. Manea ⁶³, V. Manko ¹³⁹, A.K. Manna⁴⁸, F. Manso ¹²⁵, G. Mantzaridis ⁹⁴, V. Manzari ⁵⁰, Y. Mao ⁶, R.W. Marcjan ², G.V. Margagliotti ²³, A. Margotti ⁵¹, A. Marín ⁹⁶, C. Markert ¹⁰⁷, P. Martinengo ³², M.I. Martínez ⁴⁴, G. Martínez García ¹⁰², M.P.P. Martins ^{32,109}, S. Masciocchi ⁹⁶, M. Masera ²⁴, A. Masoni ⁵², L. Massacrier ¹²⁹, O. Massen ⁵⁹, A. Mastroserio ^{130,50}, L. Mattei ^{24,125}, S. Mattiuzzo ²⁷, A. Matyja ¹⁰⁶, F. Mazzaschi ³², M. Mazzilli ^{31,114}, Y. Melikyan ⁴³, M. Melo ¹⁰⁹, A. Menchaca-Rocha ⁶⁷, J.E.M. Mendez ⁶⁵, E. Meninno ¹⁰¹, A.S. Menon ¹¹⁴, M.W. Menzel^{32,93}, M. Meres ¹³, L. Micheletti ⁵⁶, D. Mihai¹¹², D.L. Mihaylov ⁹⁴, A.U. Mikalsen ²⁰, K. Mikhaylov ^{140,139}, L. Millot ⁷², N. Minafra ¹¹⁶, D. Miśkowiec ⁹⁶, A. Modak ^{57,132}, B. Mohanty ⁷⁹, M. Mohisin Khan ^{VII,15}, M.A. Molander ⁴³, M.M. Mondal ⁷⁹, S. Monira ¹³⁴, D.A. Moreira De Godoy ¹²⁴, A. Morsch ³², T. Mrnjavac ³², S. Mrozinski ⁶⁴, V. Muccifora ⁴⁹, S. Muhuri ¹³³, A. Mulliri ²², M.G. Munhoz ¹⁰⁹, R.H. Munzer ⁶⁴, H. Murakami ¹²², L. Musa ³², J. Musinsky ⁶⁰, J.W. Myrcha ¹³⁴, N.B. Sundstrom ⁵⁹, B. Naik ¹²¹, A.I. Nambrath ¹⁸, B.K. Nandi ⁴⁷, R. Nania ⁵¹, E. Nappi ⁵⁰, A.F. Nassirpour ¹⁷, V. Nastase¹¹², A. Nath ⁹³, N.F. Nathanson ⁸², C. Nattrass ¹²⁰, K. Naumov¹⁸, A. Neagu¹⁹, L. Nellen ⁶⁵, R. Nepeivoda ⁷⁴, S. Nese ¹⁹, N. Nicassio ³¹, B.S. Nielsen ⁸², E.G. Nielsen ⁸², S. Nikolaev ¹³⁹, V. Nikulin ¹³⁹, F. Noferini ⁵¹, S. Noh ¹², P. Nomokonov ¹⁴⁰, J. Norman ¹¹⁷, N. Novitzky ⁸⁶, J. Nystrand ²⁰, M.R. Ockleton¹¹⁷, M. Ogino ⁷⁵, S. Oh ¹⁷, A. Ohlson ⁷⁴, M. Oida ⁹¹, V.A. Okorokov ¹³⁹, J. Oleniacz ¹³⁴, C. Oppedisano ⁵⁶, A. Ortiz Velasquez ⁶⁵, H. Osanai⁷⁵, J. Otwinowski ¹⁰⁶, M. Oya⁹¹, K. Oyama ⁷⁵, S. Padhan ⁴⁷, D. Pagano ^{132,55}, G. Paić ⁶⁵, S. Paisano-Guzmán ⁴⁴, A. Palasciano ⁵⁰, I. Panasenko ⁷⁴, S. Panebianco ¹²⁸, P. Panigrahi ⁴⁷,

- C. Pantouvakis ²⁷, H. Park ¹²³, J. Park ¹²³, S. Park ¹⁰³, T.Y. Park ¹³⁸, J.E. Parkkila ¹³⁴, P.B. Pati ⁸², Y. Patley ⁴⁷, R.N. Patra⁵⁰, P. Paudel¹¹⁶, B. Paul ¹³³, H. Pei ⁶, T. Peitzmann ⁵⁹, X. Peng ¹¹, M. Pennisi ²⁴, S. Perciballi ²⁴, D. Peresunko ¹³⁹, G.M. Perez ⁷, Y. Pestov¹³⁹, M. Petrovici ⁴⁵, S. Piano ⁵⁷, M. Pikna ¹³, P. Pillot ¹⁰², O. Pinazza ^{51,32}, L. Pinsky¹¹⁴, C. Pinto ³², S. Pisano ⁴⁹, M. Płoskoń ⁷³, M. Planinic ⁸⁸, D.K. Plociennik ², M.G. Poghosyan ⁸⁶, B. Polichtchouk ¹³⁹, S. Politano ^{32,24}, N. Poljak ⁸⁸, A. Pop ⁴⁵, S. Porteboeuf-Houssais ¹²⁵, I.Y. Pozos ⁴⁴, K.K. Pradhan ⁴⁸, S.K. Prasad ⁴, S. Prasad ⁴⁸, R. Preghenella ⁵¹, F. Prino ⁵⁶, C.A. Pruneau ¹³⁵, I. Pshenichnov ¹³⁹, M. Puccio ³², S. Pucillo ^{28,24}, L. Quaglia ²⁴, A.M.K. Radhakrishnan ⁴⁸, S. Ragoni ¹⁴, A. Rai ¹³⁶, A. Rakotozafindrabe ¹²⁸, N. Ramasubramanian¹²⁶, L. Ramello ^{131,56}, C.O. Ramírez-Álvarez ⁴⁴, M. Rasa ²⁶, S.S. Räsänen ⁴³, R. Rath ⁹⁶, M.P. Rauch ²⁰, I. Ravasenga ³², K.F. Read ^{86,120}, C. Reckziegel ¹¹¹, A.R. Redelbach ³⁸, K. Redlich ^{VIII,78}, C.A. Reetz ⁹⁶, H.D. Regules-Medel ⁴⁴, A. Rehman ²⁰, F. Reidt ³², H.A. Reme-Ness ³⁷, K. Reygers ⁹³, R. Ricci ²⁸, M. Richter ²⁰, A.A. Riedel ⁹⁴, W. Riegler ³², A.G. Rifferto ²⁴, M. Rignanese ²⁷, C. Ripoli ²⁸, C. Ristea ⁶³, M.V. Rodriguez ³², M. Rodríguez Cahuantzi ⁴⁴, K. Røed ¹⁹, R. Rogalev ¹³⁹, E. Rogochaya ¹⁴⁰, D. Rohr ³², D. Röhrich ²⁰, S. Rojas Torres ³⁴, P.S. Rokita ¹³⁴, G. Romanenko ²⁵, F. Ronchetti ³², D. Rosales Herrera ⁴⁴, E.D. Rosas⁶⁵, K. Roslon ¹³⁴, A. Rossi ⁵⁴, A. Roy ⁴⁸, S. Roy ⁴⁷, N. Rubini ⁵¹, J.A. Rudolph⁸³, D. Ruggiano ¹³⁴, R. Rui ²³, P.G. Russek ², R. Russo ⁸³, A. Rustamov ⁸⁰, Y. Ryabov ¹³⁹, A. Rybicki ¹⁰⁶, L.C.V. Ryder ¹¹⁶, G. Ryu ⁷¹, J. Ryu ¹⁶, W. Rzesz ¹³⁴, B. Sabiu ⁵¹, R. Sadek ⁷³, S. Sadhu ⁴², S. Sadovsky ¹³⁹, S. Saha ⁷⁹, B. Sahoo ⁴⁸, R. Sahoo ⁴⁸, D. Sahu ⁴⁸, P.K. Sahu ⁶¹, J. Saini ¹³³, K. Sajdakova³⁶, S. Sakai ¹²³, S. Sambyal ⁹⁰, D. Samitz ¹⁰¹, I. Sanna ^{32,94}, T.B. Saramela¹⁰⁹, D. Sarkar ⁸², P. Sarma ⁴¹, V. Sarritzu ²², V.M. Sarti ⁹⁴, M.H.P. Sas ³², S. Sawan ⁷⁹, E. Scapparone ⁵¹, J. Schambach ⁸⁶, H.S. Scheid ³², C. Schiaua ⁴⁵, R. Schicker ⁹³, F. Schlepper ^{32,93}, A. Schmah ⁹⁶, C. Schmidt ⁹⁶, M.O. Schmidt ³², M. Schmidt⁹², N.V. Schmidt ⁸⁶, A.R. Schmier ¹²⁰, J. Schoengarth ⁶⁴, R. Schotter ¹⁰¹, A. Schröter ³⁸, J. Schukraft ³², K. Schweda ⁹⁶, G. Scioli ²⁵, E. Scomparin ⁵⁶, J.E. Seger ¹⁴, Y. Sekiguchi¹²², D. Sekihata ¹²², M. Selina ⁸³, I. Selyuzhenkov ⁹⁶, S. Senyukov ¹²⁷, J.J. Seo ⁹³, D. Serebryakov ¹³⁹, L. Serkin ^{IX,65}, L. Šerkšnytė ⁹⁴, A. Sevcenco ⁶³, T.J. Shaba ⁶⁸, A. Shabetai ¹⁰², R. Shahoyan ³², B. Sharma ⁹⁰, D. Sharma ⁴⁷, H. Sharma ⁵⁴, M. Sharma ⁹⁰, S. Sharma ⁹⁰, T. Sharma ⁴¹, U. Sharma ⁹⁰, A. Shatat ¹²⁹, O. Sheibani¹³⁵, K. Shigaki ⁹¹, M. Shimomura ⁷⁶, S. Shirinkin ¹³⁹, Q. Shou ³⁹, Y. Sibirjak ¹³⁹, S. Siddhanta ⁵², T. Siemiaczuk ⁷⁸, T.F. Silva ¹⁰⁹, W.D. Silva ^{I,109}, D. Silvermyr ⁷⁴, T. Simantathammakul ¹⁰⁴, R. Simeonov ³⁵, B. Singh⁹⁰, B. Singh ⁹⁴, K. Singh ⁴⁸, R. Singh ⁷⁹, R. Singh ^{54,96}, S. Singh ¹⁵, V.K. Singh ¹³³, V. Singhal ¹³³, T. Sinha ⁹⁸, B. Sitar ¹³, M. Sitta ^{131,56}, T.B. Skaali ¹⁹, G. Skorodumovs ⁹³, N. Smirnov ¹³⁶, R.J.M. Snellings ⁵⁹, E.H. Solheim ¹⁹, C. Sonnabend ^{32,96}, J.M. Sonneveld ⁸³, F. Soramel ²⁷, A.B. Soto-Hernandez ⁸⁷, R. Spijkers ⁸³, I. Sputowska ¹⁰⁶, J. Staa ⁷⁴, J. Stachel ⁹³, I. Stan ⁶³, T. Stellhorn ¹²⁴, S.F. Stiefelmaier ⁹³, D. Stocco ¹⁰², I. Storehaug ¹⁹, N.J. Strangmann ⁶⁴, P. Stratmann ¹²⁴, S. Strazzi ²⁵, A. Sturniolo ^{30,53}, A.A.P. Suade ¹⁰⁹, C. Suire ¹²⁹, A. Suiu ^{32,112}, M. Sukhanov ¹⁴⁰, M. Suljic ³², R. Sultanov ¹³⁹, V. Sumberia ⁹⁰, S. Sumowidagdo ⁸¹, L.H. Tabares ⁷, S.F. Taghavi ⁹⁴, J. Takahashi ¹¹⁰, G.J. Tambave ⁷⁹, Z. Tang ¹¹⁸, J. Tanwar ⁸⁹, J.D. Tapia Takaki ¹¹⁶, N. Tapus ¹¹², L.A. Tarasovicova ³⁶, M.G. Tarzila ⁴⁵, A. Tauro ³², A. Tavira García ¹²⁹, G. Tejeda Muñoz ⁴⁴, L. Terlizzi ²⁴, C. Terrevoli ⁵⁰, D. Thakur ²⁴, S. Thakur ⁴, M. Thogersen ¹⁹, D. Thomas ¹⁰⁷, N. Tiltmann ^{32,124}, A.R. Timmins ¹¹⁴, A. Toia ⁶⁴, R. Tokumoto⁹¹, S. Tomassini ²⁵, K. Tomohiro⁹¹, N. Topilskaya ¹³⁹, M. Toppi ⁴⁹, V.V. Torres ¹⁰², A. Trifiró ^{30,53}, T. Triloiki ⁹⁵, A.S. Triolo ^{32,53}, S. Tripathy ³², T. Tripathy ¹²⁵, S. Trogolo ²⁴, V. Trubnikov ³, W.H. Trzaska ¹¹⁵, T.P. Trzciński ¹³⁴, C. Tsolanta ¹⁹, R. Tu ³⁹, A. Tumkin ¹³⁹, R. Turrisi ⁵⁴, T.S. Tveter ¹⁹, K. Ullaland ²⁰, B. Ulukutlu ⁹⁴, S. Upadhyaya ¹⁰⁶, A. Uras ¹²⁶, M. Urioni ²³, G.L. Usai ²², M. Vaid⁹⁰, M. Vala ³⁶, N. Valle ⁵⁵, L.V.R. van Doremalen⁵⁹, M. van Leeuwen ⁸³, C.A. van Veen ⁹³, R.J.G. van Weelden ⁸³, D. Varga ⁴⁶, Z. Varga ¹³⁶, P. Vargas Torres⁶⁵, M. Vasileiou ⁷⁷, A. Vasiliev ^{I,139}, O. Vázquez Doce ⁴⁹, O. Vazquez Rueda ¹¹⁴, V. Vechernin ¹³⁹, P. Veen ¹²⁸, E. Vercellin ²⁴, R. Verma ⁴⁷, R. Vértesi ⁴⁶, M. Verweij ⁵⁹, L. Vickovic³³, Z. Vilakazi¹²¹, O. Villalobos Baillie ⁹⁹, A. Villani ²³, A. Vinogradov ¹³⁹, T. Virgili ²⁸, M.M.O. Virta ¹¹⁵, A. Vodopyanov ¹⁴⁰, B. Volkel ³², M.A. Völkli ⁹⁹, S.A. Voloshin ¹³⁵, G. Volpe ³¹, B. von Haller ³², I. Vorobyev ³², N. Vozniuk ¹⁴⁰, J. Vrláková ³⁶, J. Wan ³⁹, C. Wang ³⁹, D. Wang ³⁹, Y. Wang ³⁹, Y. Wang ⁶, Z. Wang ³⁹, A. Wegrzynek ³², F. Weiglhofer ^{32,38}, S.C. Wenzel ³², J.P. Wessels ¹²⁴, P.K. Wiacek ², J. Wiechula ⁶⁴, J. Wikne ¹⁹, G. Wilk ⁷⁸, J. Wilkinson ⁹⁶, G.A. Willems ¹²⁴, B. Windelband ⁹³, M. Winn ¹²⁸, J. Witte ⁹⁶, M. Wojnar ², J.R. Wright ¹⁰⁷, C.-T. Wu ^{6,27}, W. Wu ³⁹, Y. Wu ¹¹⁸, K. Xiong ³⁹, Z. Xiong ¹¹⁸, L. Xu ^{126,6}, R. Xu ⁶, A. Yadav ⁴², A.K. Yadav ¹³³, Y. Yamaguchi ⁹¹, S. Yang ⁵⁸, S. Yang ²⁰, S. Yano ⁹¹, E.R. Yeats¹⁸, J. Yi ⁶, R. Yin ³⁹,

Z. Yin ⁶, I.-K. Yoo ¹⁶, J.H. Yoon ⁵⁸, H. Yu ¹², S. Yuan²⁰, A. Yuncu ⁹³, V. Zaccolo ²³, C. Zampolli ³², F. Zanone ⁹³, N. Zardoshti ³², P. Závada ⁶², B. Zhang ⁹³, C. Zhang ¹²⁸, L. Zhang ³⁹, M. Zhang ^{125,6}, M. Zhang ^{27,6}, S. Zhang ³⁹, X. Zhang ⁶, Y. Zhang¹¹⁸, Y. Zhang ¹¹⁸, Z. Zhang ⁶, M. Zhao ¹⁰, V. Zherebchevskii ¹³⁹, Y. Zhi¹⁰, D. Zhou ⁶, Y. Zhou ⁸², J. Zhu ³⁹, S. Zhu^{96,118}, Y. Zhu⁶, S.C. Zugravel ⁵⁶, N. Zurlo ^{132,55}

Affiliation Notes

^I Deceased

^{II} Also at: Max-Planck-Institut fur Physik, Munich, Germany

^{III} Also at: Czech Technical University in Prague (CZ)

^{IV} Also at: Italian National Agency for New Technologies, Energy and Sustainable Economic Development (ENEA), Bologna, Italy

^V Also at: Instituto de Fisica da Universidade de Sao Paulo

^{VI} Also at: Dipartimento DET del Politecnico di Torino, Turin, Italy

^{VII} Also at: Department of Applied Physics, Aligarh Muslim University, Aligarh, India

^{VIII} Also at: Institute of Theoretical Physics, University of Wroclaw, Poland

^{IX} Also at: Facultad de Ciencias, Universidad Nacional Autónoma de México, Mexico City, Mexico

Collaboration Institutes

¹ A.I. Alikhanyan National Science Laboratory (Yerevan Physics Institute) Foundation, Yerevan, Armenia

² AGH University of Krakow, Cracow, Poland

³ Bogolyubov Institute for Theoretical Physics, National Academy of Sciences of Ukraine, Kyiv, Ukraine

⁴ Bose Institute, Department of Physics and Centre for Astroparticle Physics and Space Science (CAPSS), Kolkata, India

⁵ California Polytechnic State University, San Luis Obispo, California, United States

⁶ Central China Normal University, Wuhan, China

⁷ Centro de Aplicaciones Tecnológicas y Desarrollo Nuclear (CEADEN), Havana, Cuba

⁸ Centro de Investigación y de Estudios Avanzados (CINVESTAV), Mexico City and Mérida, Mexico

⁹ Chicago State University, Chicago, Illinois, United States

¹⁰ China Nuclear Data Center, China Institute of Atomic Energy, Beijing, China

¹¹ China University of Geosciences, Wuhan, China

¹² Chungbuk National University, Cheongju, Republic of Korea

¹³ Comenius University Bratislava, Faculty of Mathematics, Physics and Informatics, Bratislava, Slovak Republic

¹⁴ Creighton University, Omaha, Nebraska, United States

¹⁵ Department of Physics, Aligarh Muslim University, Aligarh, India

¹⁶ Department of Physics, Pusan National University, Pusan, Republic of Korea

¹⁷ Department of Physics, Sejong University, Seoul, Republic of Korea

¹⁸ Department of Physics, University of California, Berkeley, California, United States

¹⁹ Department of Physics, University of Oslo, Oslo, Norway

²⁰ Department of Physics and Technology, University of Bergen, Bergen, Norway

²¹ Dipartimento di Fisica, Università di Pavia, Pavia, Italy

²² Dipartimento di Fisica dell’Università and Sezione INFN, Cagliari, Italy

²³ Dipartimento di Fisica dell’Università and Sezione INFN, Trieste, Italy

²⁴ Dipartimento di Fisica dell’Università and Sezione INFN, Turin, Italy

²⁵ Dipartimento di Fisica e Astronomia dell’Università and Sezione INFN, Bologna, Italy

²⁶ Dipartimento di Fisica e Astronomia dell’Università and Sezione INFN, Catania, Italy

²⁷ Dipartimento di Fisica e Astronomia dell’Università and Sezione INFN, Padova, Italy

²⁸ Dipartimento di Fisica ‘E.R. Caianiello’ dell’Università and Gruppo Collegato INFN, Salerno, Italy

²⁹ Dipartimento DISAT del Politecnico and Sezione INFN, Turin, Italy

³⁰ Dipartimento di Scienze MIFT, Università di Messina, Messina, Italy

³¹ Dipartimento Interateneo di Fisica ‘M. Merlin’ and Sezione INFN, Bari, Italy

³² European Organization for Nuclear Research (CERN), Geneva, Switzerland

³³ Faculty of Electrical Engineering, Mechanical Engineering and Naval Architecture, University of Split, Split, Croatia

- ³⁴ Faculty of Nuclear Sciences and Physical Engineering, Czech Technical University in Prague, Prague, Czech Republic
- ³⁵ Faculty of Physics, Sofia University, Sofia, Bulgaria
- ³⁶ Faculty of Science, P.J. Šafárik University, Košice, Slovak Republic
- ³⁷ Faculty of Technology, Environmental and Social Sciences, Bergen, Norway
- ³⁸ Frankfurt Institute for Advanced Studies, Johann Wolfgang Goethe-Universität Frankfurt, Frankfurt, Germany
- ³⁹ Fudan University, Shanghai, China
- ⁴⁰ Gangneung-Wonju National University, Gangneung, Republic of Korea
- ⁴¹ Gauhati University, Department of Physics, Guwahati, India
- ⁴² Helmholtz-Institut für Strahlen- und Kernphysik, Rheinische Friedrich-Wilhelms-Universität Bonn, Bonn, Germany
- ⁴³ Helsinki Institute of Physics (HIP), Helsinki, Finland
- ⁴⁴ High Energy Physics Group, Universidad Autónoma de Puebla, Puebla, Mexico
- ⁴⁵ Horia Hulubei National Institute of Physics and Nuclear Engineering, Bucharest, Romania
- ⁴⁶ HUN-REN Wigner Research Centre for Physics, Budapest, Hungary
- ⁴⁷ Indian Institute of Technology Bombay (IIT), Mumbai, India
- ⁴⁸ Indian Institute of Technology Indore, Indore, India
- ⁴⁹ INFN, Laboratori Nazionali di Frascati, Frascati, Italy
- ⁵⁰ INFN, Sezione di Bari, Bari, Italy
- ⁵¹ INFN, Sezione di Bologna, Bologna, Italy
- ⁵² INFN, Sezione di Cagliari, Cagliari, Italy
- ⁵³ INFN, Sezione di Catania, Catania, Italy
- ⁵⁴ INFN, Sezione di Padova, Padova, Italy
- ⁵⁵ INFN, Sezione di Pavia, Pavia, Italy
- ⁵⁶ INFN, Sezione di Torino, Turin, Italy
- ⁵⁷ INFN, Sezione di Trieste, Trieste, Italy
- ⁵⁸ Inha University, Incheon, Republic of Korea
- ⁵⁹ Institute for Gravitational and Subatomic Physics (GRASP), Utrecht University/Nikhef, Utrecht, Netherlands
- ⁶⁰ Institute of Experimental Physics, Slovak Academy of Sciences, Košice, Slovak Republic
- ⁶¹ Institute of Physics, Homi Bhabha National Institute, Bhubaneswar, India
- ⁶² Institute of Physics of the Czech Academy of Sciences, Prague, Czech Republic
- ⁶³ Institute of Space Science (ISS), Bucharest, Romania
- ⁶⁴ Institut für Kernphysik, Johann Wolfgang Goethe-Universität Frankfurt, Frankfurt, Germany
- ⁶⁵ Instituto de Ciencias Nucleares, Universidad Nacional Autónoma de México, Mexico City, Mexico
- ⁶⁶ Instituto de Física, Universidade Federal do Rio Grande do Sul (UFRGS), Porto Alegre, Brazil
- ⁶⁷ Instituto de Física, Universidad Nacional Autónoma de México, Mexico City, Mexico
- ⁶⁸ iThemba LABS, National Research Foundation, Somerset West, South Africa
- ⁶⁹ Jeonbuk National University, Jeonju, Republic of Korea
- ⁷⁰ Johann-Wolfgang-Goethe Universität Frankfurt Institut für Informatik, Fachbereich Informatik und Mathematik, Frankfurt, Germany
- ⁷¹ Korea Institute of Science and Technology Information, Daejeon, Republic of Korea
- ⁷² Laboratoire de Physique Subatomique et de Cosmologie, Université Grenoble-Alpes, CNRS-IN2P3, Grenoble, France
- ⁷³ Lawrence Berkeley National Laboratory, Berkeley, California, United States
- ⁷⁴ Lund University Department of Physics, Division of Particle Physics, Lund, Sweden
- ⁷⁵ Nagasaki Institute of Applied Science, Nagasaki, Japan
- ⁷⁶ Nara Women's University (NWU), Nara, Japan
- ⁷⁷ National and Kapodistrian University of Athens, School of Science, Department of Physics , Athens, Greece
- ⁷⁸ National Centre for Nuclear Research, Warsaw, Poland
- ⁷⁹ National Institute of Science Education and Research, Homi Bhabha National Institute, Jatni, India
- ⁸⁰ National Nuclear Research Center, Baku, Azerbaijan
- ⁸¹ National Research and Innovation Agency - BRIN, Jakarta, Indonesia
- ⁸² Niels Bohr Institute, University of Copenhagen, Copenhagen, Denmark
- ⁸³ Nikhef, National institute for subatomic physics, Amsterdam, Netherlands
- ⁸⁴ Nuclear Physics Group, STFC Daresbury Laboratory, Daresbury, United Kingdom
- ⁸⁵ Nuclear Physics Institute of the Czech Academy of Sciences, Husinec-Řež, Czech Republic

- ⁸⁶ Oak Ridge National Laboratory, Oak Ridge, Tennessee, United States
⁸⁷ Ohio State University, Columbus, Ohio, United States
⁸⁸ Physics department, Faculty of science, University of Zagreb, Zagreb, Croatia
⁸⁹ Physics Department, Panjab University, Chandigarh, India
⁹⁰ Physics Department, University of Jammu, Jammu, India
⁹¹ Physics Program and International Institute for Sustainability with Knotted Chiral Meta Matter (WPI-SKCM²), Hiroshima University, Hiroshima, Japan
⁹² Physikalischs Institut, Eberhard-Karls-Universität Tübingen, Tübingen, Germany
⁹³ Physikalischs Institut, Ruprecht-Karls-Universität Heidelberg, Heidelberg, Germany
⁹⁴ Physik Department, Technische Universität München, Munich, Germany
⁹⁵ Politecnico di Bari and Sezione INFN, Bari, Italy
⁹⁶ Research Division and ExtreMe Matter Institute EMMI, GSI Helmholtzzentrum für Schwerionenforschung GmbH, Darmstadt, Germany
⁹⁷ Saga University, Saga, Japan
⁹⁸ Saha Institute of Nuclear Physics, Homi Bhabha National Institute, Kolkata, India
⁹⁹ School of Physics and Astronomy, University of Birmingham, Birmingham, United Kingdom
¹⁰⁰ Sección Física, Departamento de Ciencias, Pontificia Universidad Católica del Perú, Lima, Peru
¹⁰¹ Stefan Meyer Institut für Subatomare Physik (SMI), Vienna, Austria
¹⁰² SUBATECH, IMT Atlantique, Nantes Université, CNRS-IN2P3, Nantes, France
¹⁰³ Sungkyunkwan University, Suwon City, Republic of Korea
¹⁰⁴ Suranaree University of Technology, Nakhon Ratchasima, Thailand
¹⁰⁵ Technical University of Košice, Košice, Slovak Republic
¹⁰⁶ The Henryk Niewodniczanski Institute of Nuclear Physics, Polish Academy of Sciences, Cracow, Poland
¹⁰⁷ The University of Texas at Austin, Austin, Texas, United States
¹⁰⁸ Universidad Autónoma de Sinaloa, Culiacán, Mexico
¹⁰⁹ Universidade de São Paulo (USP), São Paulo, Brazil
¹¹⁰ Universidade Estadual de Campinas (UNICAMP), Campinas, Brazil
¹¹¹ Universidade Federal do ABC, Santo Andre, Brazil
¹¹² Universitatea Nationala de Stiinta si Tehnologie Politehnica Bucuresti, Bucharest, Romania
¹¹³ University of Derby, Derby, United Kingdom
¹¹⁴ University of Houston, Houston, Texas, United States
¹¹⁵ University of Jyväskylä, Jyväskylä, Finland
¹¹⁶ University of Kansas, Lawrence, Kansas, United States
¹¹⁷ University of Liverpool, Liverpool, United Kingdom
¹¹⁸ University of Science and Technology of China, Hefei, China
¹¹⁹ University of South-Eastern Norway, Kongsberg, Norway
¹²⁰ University of Tennessee, Knoxville, Tennessee, United States
¹²¹ University of the Witwatersrand, Johannesburg, South Africa
¹²² University of Tokyo, Tokyo, Japan
¹²³ University of Tsukuba, Tsukuba, Japan
¹²⁴ Universität Münster, Institut für Kernphysik, Münster, Germany
¹²⁵ Université Clermont Auvergne, CNRS/IN2P3, LPC, Clermont-Ferrand, France
¹²⁶ Université de Lyon, CNRS/IN2P3, Institut de Physique des 2 Infinis de Lyon, Lyon, France
¹²⁷ Université de Strasbourg, CNRS, IPHC UMR 7178, F-67000 Strasbourg, France, Strasbourg, France
¹²⁸ Université Paris-Saclay, Centre d'Etudes de Saclay (CEA), IRFU, Département de Physique Nucléaire (DPhN), Saclay, France
¹²⁹ Université Paris-Saclay, CNRS/IN2P3, IJCLab, Orsay, France
¹³⁰ Università degli Studi di Foggia, Foggia, Italy
¹³¹ Università del Piemonte Orientale, Vercelli, Italy
¹³² Università di Brescia, Brescia, Italy
¹³³ Variable Energy Cyclotron Centre, Homi Bhabha National Institute, Kolkata, India
¹³⁴ Warsaw University of Technology, Warsaw, Poland
¹³⁵ Wayne State University, Detroit, Michigan, United States
¹³⁶ Yale University, New Haven, Connecticut, United States
¹³⁷ Yildiz Technical University, Istanbul, Turkey
¹³⁸ Yonsei University, Seoul, Republic of Korea

¹³⁹ Affiliated with an institute formerly covered by a cooperation agreement with CERN

¹⁴⁰ Affiliated with an international laboratory covered by a cooperation agreement with CERN.